Thesis for the Degree of Licentiate of Engineering

Constellation Shaping in Optical Communication Systems

Ali Mirani

CHALMERS

Photonics Laboratory
Department of Microtechnology and Nanoscience - MC2
Chalmers University of Technology
Göteborg, Sweden, 2021

Constellation Shaping in Optical Communication Systems
Ali Mirani
Göteborg, February 2021

Chalmers University of Technology
Microtechnology and Nanoscience - MC2
Photonics Laboratory
SE-412 96 Göteborg, Sweden
Phone: +46 (0) 31 772 1000

ISSN 1652-0769
Technical Report MC2-439

Printed in Sweden by Reproservice, Chalmers University of Technology
Göteborg, Sweden, February 2021

Constellation Shaping in Optical Communication Systems

Ali Mirani
Photonics Laboratory
Department of Microtechnology and Nanoscience - MC2
Chalmers University of Technology

Abstract

Exploiting the full-dimensional capacity of coherent optical communication systems is needed to overcome the increasing bandwidth demands of the future Internet. To achieve capacity, both coding and shaping gains are required, and they are, in principle, independent. Therefore it makes sense to study shaping and how it can be achieved in various dimensions and how various shaping schemes affect the whole performance in real systems. This thesis investigates the performance of constellation shaping methods including geometric shaping (GS) and probabilistic shaping (PS) in coherent fiber-optic systems.

To study GS, instead of considering machine learning approaches or optimization of irregular constellations in two dimensions, we have explored multidimensional lattice-based constellations. These constellations provide a regular structure with a fast and low-complexity encoding and decoding. In simulations, we show the possibility of transmitting and detecting constellation with a size of more than 10^{28} points which can be done without a look-up table to store the constellation points. Moreover, improved performance in terms of bit error rate, symbol error rate, and transmission reach are demonstrated over the linear additive white Gaussian noise as well as the nonlinear fiber channel compared to QAM formats.

Furthermore, we investigate the performance of PS in two separate scenarios, i.e., transmitter impairments and transmission over hybrid systems with on-off keying channels. In both cases, we find that while PS-QAM outperforms the uniform QAM in the linear regime, uniform QAM can achieve better performance at the optimum power in the presence of transmitter or channel nonlinearities.

Keywords: optical communications, coherent receiver, constellation shaping, multidimensional modulation format, geometric shaping, probabilistic shaping

Publications

This thesis is based on the work contained in the following papers:

[A] **Ali Mirani**, Erik Agrell, and Magnus Karlsson, "Low-complexity geometric shaping", *Journal of Lightwave Technology*, vol. 39, no. 2, pp. 363-371, Jan 2021.
DOI: 10.1109/JLT.2020.3033031.

[B] **Ali Mirani**, Erik Agrell, and Magnus Karlsson, "Lattice-based geometric shaping", in *European Conference on Optical Communication (ECOC)*, Brussels, Belgium, Dec 2020.
DOI: 10.1109/ECOC48923.2020.9333162

[C] **Ali Mirani**, Mikael Mazur, Erik Agrell, Benjamin Foo, Jochen Schröder, Peter Andrekson, and Magnus Karlsson, "Comparison of uniform cross QAM and probabilistically shaped QAM formats under the impact of transmitter impairments", in *European Conference on Optical Communication (ECOC)*, Dublin, Ireland, Sep 2019.
DOI: 10.1049/cp.2019.0994

[D] Diego Villafani, **Ali Mirani**, Henrik Åhlfeldt, Jochen Schröder, Magnus Karlsson, and Peter Andrekson, "Performance of Probabilistic Shaping Coherent Channels in Hybrid Systems", in *International Conference on Transparent Optical Networks (ICTON)*, Bari, Italy, July 2020.
DOI: 10.1109/ICTON51198.2020.9203055

Other publications by the author, not included in this thesis, are:

[E] Lars Lundberg, Mikael Mazur, **Ali Mirani**, Benjamin Foo, Jochen Schröder, Victor Torres-Company, Magnus Karlsson, and Peter Andrekson, "Phase-coherent lightwave communications with frequency combs", *Nature Communications* 11, 201 (2020). https://doi.org/10.1038/s41467-019-14010-7.

[F] Diego Villafani, **Ali Mirani**, Xiaodan Pang, Edgard Goobar, Jochen Schröder, Magnus Karlsson, and Peter Andrekson, "Phase Noise Characterization and EEPN of a Full C-Band Tunable Laser in Coherent Optical Systems", *IEEE Photonics Technology Letters*, vol. 31, no. 24, pp. 1991-1994, Dec 2019. DOI: 10.1109/LPT.2019.2952816

Contents

Acknowledgement

First and foremost, I would like to thank my supervisor, Prof. Magnus Karlsson, for giving me the opportunity to pursue my PhD in the Photonics group and sharing all your deep knowledge on optics. I would like to thank my co-supervisor, Prof. Erik Agrell, for all the fruitful discussions and your valuable feedback to improve my writing skills. Special thanks to my examiner, Prof. Peter Andrekson, for managing the lab duties and reminding me of the importance of experimental work.

Dr. Jochen Schröder, Dr. Mikael Mazur, and Dr. Ben Foo deserve special thanks for introducing and helping me with Python programming and sharing your knowledge on fiber-optic communications. Many thanks to Dr. Diego Villafani for the interesting collaborations and discussions in the lab. Special thanks to Dr. Lars Lundberg to involve me in your phase tracking experiment to understand more about optical coherent systems. Thanks to Dr. Attila Fülöp, Dr. Henrick Eliasson, and Dr. Emanuel Haglund for the short but inspiring overlap in our PhD studies. I wish to thank Dr. Ravikiran Kakarla and Kovendhan Vijayan for all the friendly discussions and all the experimental knowledge you have taught me. Special thanks to Isra and Marcello for the valuable friendship inside and outside academia. I wish to thank Shen, Ekaterina, and Zonglong for all the interesting discussions on research. Many thanks to Jeanette Träff for managing all administrative works and being a kind administrator. I would like to thank everyone at the Photonics lab for making it such a nice environment.

I would like to thank all my Iranian friends who had made Sweden feel like home. Special thanks to Kamran, Mohammad Ali, Fatemeh, Nastaran, Saeed, and Mehdi for your support during my first days in Sweden.

Last but not least, my deepest thanks go to Maryam for your love and your support in both life and work and to my parents and my sister for your ever-existed encouragement in all steps of my life.

Ali Mirani
Göteborg, February 2021

Acronyms

ADC	analog-to-digital converter
AOM	acousto-optic modulater
APE	asymptotic power efficiency
APE	in-phase and quadrature
ASE	amplified spontaneous emission
AWGN	additive white Gaussian noise
BER	bit error rate
BPSK	binary phase-shift keying
CPA	closest point algorithm
DAC	digital-to-analog converter
DSP	digital signal processing
EDFA	Erbium-doped fiber amplifier
ENOB	effective number of bits
FEC	forward error correction
GMI	generalized mutual information
GN	Gaussian noise
GS	geometric shaping
HD	hard-decision
IM/DD	intensity modulation with direct detection
MB	Maxwell-Boltzmann
MI	mutual information
MIMO	multiple-input and multiple-output
ML	maximum likelihood
MZM	Mach-Zehnder modulator

NGMI	normalized generalized mutual information
NLSE	nonlinear Schrödinger equation
OOK	on-off keying
PAS	probabilistic amplitude shaping
PS	probabilistic shaping
QAM	quadrature amplitude modulation
QPSK	quadrature phase-shift keying
RRC	root-raised-cosine
SD	soft-decision
SE	spectral efficiency
SER	symbol error rate
SNR	signal to noise ratio
SSFM	split-step Fourier method
VC	Voronoi constellation
WDM	wavelength-division multiplexing

CHAPTER 1

Introduction

In the time of writing this thesis, the Covid-19 pandemic has affected many aspects of life including education, economy, and style of living [1]. Many countries have been locking down their population and applied strict quarantine roles to control the spread of the virus. In this situation, some activities have been stopped but many others have been conducted remotely to avoid a complete global collapse [2]. Most of the world's education system has been carried out online through video streaming platforms [3]. Almost all regular conferences have been happening online to avoid traveling and physical interaction of attendees [4]. Jobs that do not depend on an official workplace have shifted to working from home and online meetings.

All these online communications have challenged the Internet network to connect people in the whole world together with the best quality possible [5, 6], e.g., high bandwidth video streaming. This emphasizes the importance of optical communication systems which are the main backbone and infrastructure of the global Internet network [7]. Without improvements in the optical communication systems, the Internet would not have been able to meet the global demands to transfer and access more data.

1.1 History

A starting point for modern optical communication systems dates back to inventions of lasers [8, 9] and low-loss optical fibers [10] after 1960. The invention of the laser brought the opportunity of utilizing a coherent and monochromatic light source to transmit the information. In 1960, the first solid ruby laser was invented by Theodore Maiman [11], the first continuously operating gas laser was invented [12] by Ali Javan, William Bennett, Jr., and Donald Herriott at Bell Labs in 1961, and in 1962, the first semiconductor diode laser was fabricated [13] by Robert N. Hall and coworkers at the General Electric Research and Development Center. Optical fibers with high attenuation and short length were used during the 1960s for gastroscopy [14]. Later, more efforts were made to reduce impurities and reduce the fiber losses from 20 dB/km in 1970 [15] to today's less than 0.2 dB/km at infrared wavelength region near 1.55 μm [10, 16, 17]. Demonstrations of commercial fiber optical transmission during the 1970s to transmit data rates of Mbit/sec over a few kilometers were another huge step for the communication community and industry [18, 19].

Another important breakthrough in optical communication was the invention of erbium-doped fiber amplifier (EDFA) in 1980s [20]. The EDFA eliminated the optical-electrical-optical repeaters, by amplifying the signal directly in the optical domain and decreasing the cost of the long-haul transmission links [21]. Moreover, because of the high bandwidth of EDFAs more channels could be simultaneously amplified and higher data rates transmitted in the same fiber [22].

Studied in the 1980s, coherent receivers were another milestone for optical communication systems. Because of the hardware complexity, they were forgotten under the shadow of optical amplifiers for almost 20 years [23]. In 2005, a coherent receiver was used to detect a polarization-multiplexed quadrature phase-shift keying (QPSK) signal in a wavelength-division multiplexing (WDM) system followed by digital signal processing (DSP) to improve the sensitivity and phase estimation [24]. This created a widespread interest in coherent optical communication systems again since it brought access to the full optical field to increase the spectral efficiency (SE) by employing multi-level modulation formats [25].

All the previous developments have been responsible to increase the data rate and transmission reach in optical communication systems. One question that remains is the ultimate capacity of the optical fibers. In

1948, Shannon showed that for any linear communication channel with an additive Gaussian noise source, the channel capacity C is determined by the available bandwidth W and the signal to noise ratio (SNR) through $C = W \log_2(1 + SNR)$ [26]. However, the optical channel is not an additive white Gaussian noise (AWGN) channel in all operation regimes. For optical channels, many efforts have been made to close the gap between the achievable information rate and the channel capacity in linear regime [27] and to find an estimate for the actual nonlinear capacity [28–30].

1.2 This thesis

The focus of this thesis is on investigating the performance of constellation shaping methods to improve the achievable information rate and the power efficiency in coherent optical communication systems. Two main approaches are geometric shaping (GS) [31, 32] and probabilistic shaping (PS) [33, 34] where the geometry and the probability distribution of constellation points are modified to improve the performance compared to quadrature amplitude modulation (QAM) formats, respectively. These methods are mainly designed for the linear AWGN channel and their performance needs to be evaluated over the nonlinear fiber channel.

The papers included in this thesis are investigating these constellation shaping methods. In [Paper A-B], the performance of the lattice-based geometric shaping method is explored in the AWGN and nonlinear fiber channels, and fast and low-complexity modulation and demodulation algorithms are presented. Constellation sizes with more than 10^{28} points are simulated without any look-up tables to store them and more than 38% reach improvement is shown compared to 4-QAM. In [Paper C], the performance of probabilistically shaped constellations are compared with the cross-QAM formats in the presence of digital-to-analog converter (DAC) and Mach-Zehnder modulator (MZM) impairments without any digital pre-compensation. We demonstrate that cross-QAM outperforms PS-QAM by a factor of up to 4 in symbol error rate and higher achievable information rates, at the same source entropy and optimal electrical signal powers. Finally, in [Paper D], the probabilistically shaped QAM formats are compared with uniform QAM in hybrid systems where on-off keying (OOK) formats are co-propagating with the higher-order modulation formats.

1.2.1 Thesis outline

The outline of this thesis is as follows. In chapter 2, the basic building blocks of a coherent communication system are introduced including the transmitter and the receiver impairments. Different channel models are presented for the fiber channel and the required signal processing algorithms are discussed to compensate for the transceiver and channel distortions. In chapter 3, the modulation formats with their properties and the possible parameters to compare different formats together are introduced. Chapter 4 discusses the constellation shaping methods including both probabilistic and geometric shaping. Finally, in chapter 5, the future outlooks are presented and chapter 6 outlines the main results in the appended papers.

CHAPTER 2

Coherent Fiber-Optic Communication Systems

The developments of the global Internet are mainly due to the improvements in fiber links which connect continents with more than thousands of kilometers distance [35–37]. Early demonstrations of optical links could carry information at Mbits/sec [38], however, today's networks have Tbits/sec capacity [39]. Multiple technologies including lasers, optical amplifiers, and high-speed electrical transceivers have made coherent optical communication systems the main infrastructure in the long-haul transmission of today. Combined with advanced DSP, coherent systems can achieve high SE [40] and be robust against channel impairments [41]. These benefits have made coherent systems dominant for long-haul networks and they are currently attracting more attention to be used in short-reach networks as well [42].

In this chapter, some of the essential building blocks of a point-to-point coherent communication system are investigated including the transmitter, fiber channel, and receiver.

2.1 Transmitter

In this section, the basic components of optical transmitters are introduced including the discrete-time signal processing, transforming discrete-time data to continuous analog electrical signal, and finally converting the electrical signal to the optical domain. A block diagram of the trans-

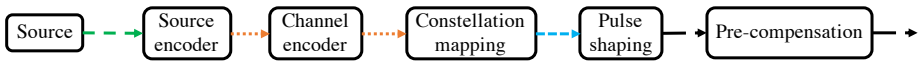

Figure 2.1: The building blocks to transform the source messages to discrete-time signal. From left to right, different arrows indicate message (green), bit (orange), discrete-time discrete-amplitude (blue), and discrete-time continuous-amplitude (black) information.

mitter side components is given in fig. 2.1.

2.1.1 Digital domain

As shown in fig. 2.1, in the first step, source messages are passed through the source encoder to remove the redundant information with an efficient representation and generate a bit stream representation. For instance, if the source outputs are the 26 English letters, instead of presenting each letter with 5 bits, it is possible to represent each letter based on their occurrence probability. The letters with higher probability will be presented with fewer bits and the letters with lower probability need more bits. This way, on average, less than 5 bits would be required to show the source outputs [43].

After source coding, the bits are affected by the channel encoding block. The channel coding makes sure that the transmission will be highly reliable by adding redundant bits [44].

The next step after preparing the bits is mapping them to symbols. These symbols are members of a set which is called a *constellation*. There are different ways to represent the symbols, e.g., complex numbers, complex vectors, or multidimensional real vectors [45, 46]. Each symbol $\mathbf{c}$ is labeled by a string of bits as $b_0 b_1 \cdots b_{m-1}$. Then, these symbols are transmitted over their corresponding time slot, polarization, frequency, or spatial mode.

Usually, the combination of channel coding and constellation mapping with an additional shaping block are used to perform constellation shaping either to change the probability distribution or Euclidean geometry of the constellation. More details about constellation shaping are discussed in chapter 4.

In the next step, discrete-time discrete-amplitude symbols $\mathbf{c}$ are carried by a discrete-time continuous-amplitude pulse $h(t)$, i.e.,

$$\mathbf{s}(t) = \sum_i \mathbf{c}_i \cdot h(t - iT), \tag{2.1}$$

where $h(t)$ is the pulse shaping function. Since using square-shaped pulses in the transmission is physically impractical, other forms of pulse shaping are required. In order to satisfy the Nyquist intersymbol interference criterion, usually, the raised cosine pulse shaping is used to transmit the symbols [47, Chap. 7]. To improve noise cancellation, this can also be done by using a root-raised-cosine (RRC) filter in the transmitter and another RRC in the receiver [48, Chap. 9]. Then, the bandwidth of the signal can be controlled by the RRC filter. The transfer function and the time domain impulse response of these filters are given as [49, 50]

$$H_{RC}(f) = \begin{cases} T & : \ 0 \leq |f| \leq \frac{1-\beta}{2T} \\ \frac{T}{2}\left\{1+\cos\left[\frac{\pi T}{\beta}\left(|f|-\frac{1-\beta}{2T}\right)\right]\right\} & : \frac{1-\beta}{2T} \leq |f| \leq \frac{1+\beta}{2T} \\ 0 & : \quad |f| > \frac{1+\beta}{2T} \end{cases} \tag{2.2}$$

$$h_{RC}(t) = \frac{\sin(\pi t/T)}{\pi t/T}\frac{\cos(\pi\beta t/T)}{1-4\beta^2 t^2/T^2} \tag{2.3}$$

$$H_{RRC}(f) = \begin{cases} \sqrt{T} & : \ 0 \leq |f| \leq \frac{1-\beta}{2T} \\ \sqrt{T}\sin\left(\frac{\pi(1+\beta-2|f|T)}{4\beta}\right) & : \frac{1-\beta}{2T} \leq |f| \leq \frac{1+\beta}{2T} \\ 0 & : \quad |f| > \frac{1+\beta}{2T} \end{cases} \tag{2.4}$$

$$h_{RRC}(t) = \frac{2\beta}{\pi\sqrt{T}}\frac{\cos((1+\beta)\pi t/T)+\sin((1-\beta)\pi t/T)/(4\beta t/T)}{1-16\beta^2 t^2/T^2}. \tag{2.5}$$

In these equations, β is the roll-off factor that can control the bandwidth of the filter and it shows the excess bandwidth beyond the Nyquist bandwidth of $1/(2T)$ where T is the symbol duration.

Finally, signal processing can also be done to pre-compensate the chromatic dispersion [51] and mitigate the nonlinear response of the fiber [52]. Moreover, the non-ideal transfer function of the transmitter components can be compensated before transferring the data to electrical and optical domains [53]. These non-ideal responses are discussed in the following sections. After pre-compensation, the discrete-time continuous-amplitude signal is ready to be converted to an continuous-time electrical waveform.

2.1.2 Digital-to-analog converter

After source and channel coding, constellation bit mapping, pulse shaping, and pre-compensation algorithms in the discrete-time domain, the

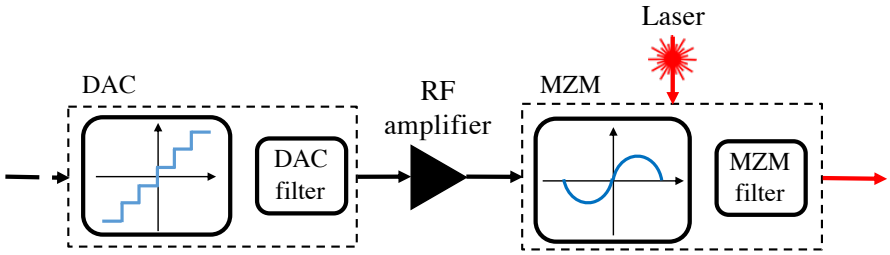

Figure 2.2: The building blocks to transform the discrete-time signal to optical waveform. The RF amplifier amplifies the electrical signal. From left to right, different arrows indicate the discrete-time signal (dashed black), continuous-time electrical signal (black), and the optical waveform (red).

data is ready to be converted to the continuous-time analog electrical domain by the DAC. The DAC is a component that converts the discrete-time signal into a continuous-time analog electrical waveform. It has a finite resolution in terms of discrete output signal levels. A sampling clock and a reference voltage are other essential parts of the DAC [54,55].

Usually, the input to the DAC is normalized between -1 and 1 and the finite resolution of the DAC quantizes the input between specific levels which correspond to the resolution. This can be represented as

$$x = Q(x) + n_q, \tag{2.6}$$

where $Q(\cdot)$ gives the quantized value of the input to the DAC and n_q is called the quantization noise with a uniform distribution which its variance depends on the DAC resolution. The range of each interval which takes the same value at the DAC output is equal to $\Delta = (1-(-1))/2^b = 2^{1-b}$ where b is the DAC resolution. The quantization noise distribution is given by $f(n_q) = (1/\Delta) \cdot \text{rect}(\Delta \cdot n_q)$ where $\text{rect}(\cdot)$ is a rectangular-shaped pulse with unit amplitude and unit domain around 0.

Other DAC impairments are the limited operation bandwidth and electrical noise and jitter. Usually, the DAC frequency response is modeled as a Bessel function [56,57]. These effects reduce the effective number of bits (ENOB) which are used to represent the signal.

2.1.3 Mach-Zehnder modulator

Converting the electrical signal after the DAC to the optical domain is the last step in the transmitter. As shown in fig. 2.2, the electrical

signal at the output of the DAC is amplified by an electrical amplifier to provide enough electrical power. The amplified signal is then fed into an optical modulator which is responsible to change the optical carrier-envelope according to this electrical signal. The optical modulator that is typically used in optical communication systems is the MZM.

An MZM is able to modulate the amplitude of the optical field, however, combining two MZMs with a $\pi/2$ phase-shift in one of the arms enables creating two orthogonal signals in which the amplitude and phase of the optical carrier can be modulated simultaneously. Performing the same procedure over two orthogonal polarization components of the optical carrier provides a four-dimensional space, in which each dimension is controlled and modulated by an MZM [58].

The relation between the output optical power and the input electrical signal of the MZM is described by a sinusoidal function. This nonlinear behavior can distort the signal if the input electrical signal has high power and is not pre-compensated in the digital domain. Usually, in the digital domain, an inverse sinusoidal function is applied to linearize the performance of the overall system [59].

The bandwidth limitation is another non-ideal characteristic of the MZM which is mainly described by a Gaussian filter with a limited bandwidth [60].

2.1.4 Laser

The carrier in the optical communication systems is light wave which is generated through the process of stimulated emission. The light source at the output of the laser is considered to be more coherent than other light sources in time and space. In coherent communication systems, it is required to have one laser at the transmitter to carry the information signal and one laser at the receiver as the local oscillator to provide the phase reference to detect the relative variations of the received signal. The output of a laser is however not an ideal sinusoidal wave with a well-defined amplitude and phase. Because of the random spontaneous emissions during the process of photon generation, there are random fluctuations in the output power and carrier phase. The single-mode laser output is then described by

$$E(t) = (A + \Delta A(t)) \cdot \sin(\omega_0 t + \phi_0 + \Delta\phi(t)), \tag{2.7}$$

where $\Delta A(t)$ and $\Delta\phi(t)$ are the fluctuations of amplitude and phase in continuous time notation, respectively. Also, A, ϕ_0, and ω_0 indicate

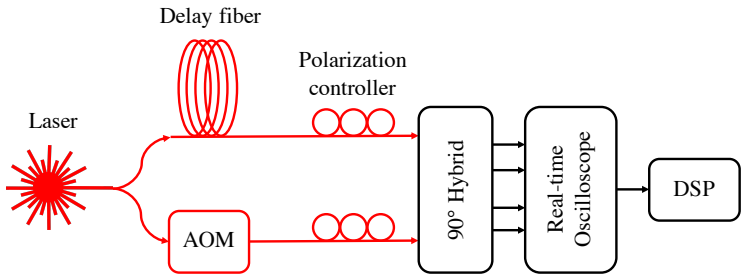

Figure 2.3: Phase noise measurement setup using coherent receiver.

the amplitude, initial phase, and angular frequency of the light. For simplicity, ϕ_0 is usually considered equal to zero and ΔA is assumed to be negligible because of the feedback control systems. However, the remaining phase perturbations of the received signal are accumulated and result in a phase noise which is described by a Wiener process [61]. In this model, the kth transmitted symbol is affected by a phase rotation of

$$\phi(k) = \phi(k-1) + \theta(k) = \sum_{m=0}^{k-1} \theta(m), \tag{2.8}$$

where $\theta(m)$ are independent Gaussian random variables with zero mean and variance $\sigma_\theta^2 = 2\pi\Delta\nu T$, with T indicating the time between the samples and $\Delta\nu$ corresponding to the total transmitter and local oscillator laser linewidths.

The laser linewidth can be measure with different methods. One way is to beat the laser output with a delayed version of itself in a coherent receiver [62]. The delay line is selected to provide uncorrelated phase variations in the detectors and needs to be much larger than the coherence time ($1/\Delta\nu$) of the laser. After detecting the photo-current with a high-speed oscilloscope, signal processing techniques can be used to estimate the laser linewidth. An example setup for this method is shown in fig. 2.3. In this setup, the laser is split into two arms. The polarization controllers are used to align the polarization states of the fields and an acousto-optic modulater (AOM) shifts the frequency up to avoid low-frequency noise in the spectrum.

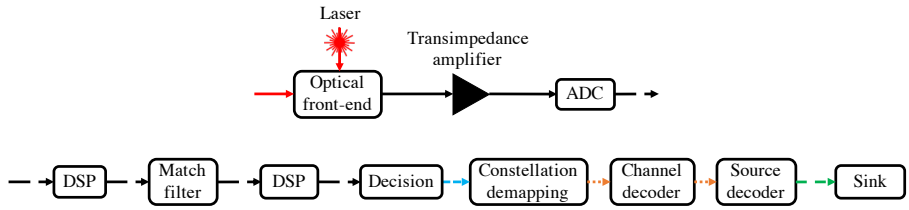

Figure 2.4: Block diagram of the optical receiver.

2.2 Receiver

As shown in fig. 2.4, on the receiver side, the inverse operations of the transmitter are applied. First, the optical signal needs to be converted to the electrical domain by the front-end block and then the electrical signal is sampled by the analog-to-digital converter (ADC) to generate the discrete-time signal. Non-ideal responses of the receiver components and some of the fiber impairments, e.g., chromatic dispersion and fiber nonlinearity, can be compensated in the first DSP block. In the next block, match filtering is applied to improve the SNR of the received signal. Other channel impairments are compensated in the second DSP block and are briefly discussed in this section. Finally, based on the received samples, the most probable transmitted constellation points are selected and demapped to generate the corresponding bit stream. In the end, channel decoding is done to correct and find the possible errors and source decoding generates the received messages.

2.2.1 Optical front-end

In modern communication systems where phase and amplitude modulations are used together to achieve higher SEs, a coherent receiver is required which consists of a local oscillator as a phase reference. The coherent receiver includes several parts shown in fig. 2.5. First, the received optical signal and local oscillator are split into two orthogonal polarizations. Then, for each polarization, the signal and local oscillator are mixed in a 90° hybrid. Then, these combined signals are detected by balanced photo-detectors. Finally, the electrical signal is sampled using an ADC and is ready to be processed in the discrete-time domain.

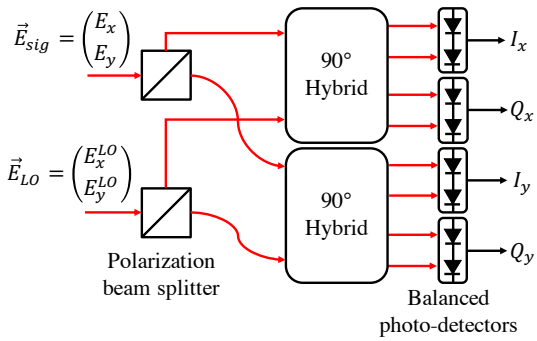

Figure 2.5: Block diagram of a front-end for a dual polarization system

2.2.2 Digital signal processing

In coherent communication systems, the most important impairments which are compensated in the discrete-time domain are the transceiver components non-ideal responses, fiber channel chromatic dispersion, timing recovery, frequency offset estimation, polarization mixing, phase tracking, and fiber nonlinearities.

Transmitter impairments can be pre-compensated in the digital domain before transmission. However, compensating for these impairments in the receiver side has also been studied which might result in channel noise enhancement compared to the pre-compensation techniques [63]. Coherent receiver impairments can also be mitigated digitally. One famous algorithm which improves the distorted signal because of quadrature imbalance is the Gram-Schmidt orthogonalization [64] procedure which fixes the non-orthogonality of in-phase and quadrature (IQ) components because of imperfections in hybrids, phase shifters, and photodiodes.

Chromatic dispersion can be compensated either in the optical domain [65] or the digital domain [66]. In the digital domain, the signal passes through an all-pass filter with a response that approximates

$$H(z,\omega) = \exp(j\omega^2\beta_2 z/2), \tag{2.9}$$

or in the time domain

$$h(z,t) = \sqrt{\frac{j}{2\pi\beta_2 z}}\exp(-jt^2/(2\beta_2 z)). \tag{2.10}$$

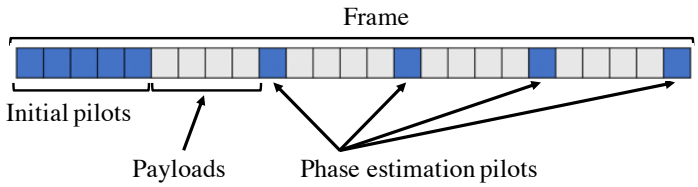

Figure 2.6: Frame structure for pilot-based DSP.

Timing recovery is the recovery of the correct symbol timing, i.e., estimating the optimal time instant to sample in the middle of the signal to capture the received symbols. Garner's feedback algorithm [67] is an example of low complexity time estimation for timing recovery.

In the front-end block, intradyne detection of the received signal by combining with a local oscillator leaves a residual continuous frequency component in the signal. After sampling, this impairment causes a linear phase walk in the received symbols and is usually compensated by removing the data modulation from the signal and finding the highest peak in the Fourier transform of the signal [68].

In order to compensate for polarization mixing and phase tracking, pilot-based DSP has been applied in this thesis. The structure of the pilot symbols and payloads are shown in fig. 2.6. The pilot symbols are all selected from a QPSK constellation and are known to the receiver. In the receiver, the received symbols are compared with the transmitted symbols and their differences are used to estimate the channel. Phase pilot symbols are inserted periodically in the frame to track the phase rotations [69].

There are also nonlinear compensation techniques that mitigate the fiber nonlinear effects. Digital backpropagation is one of the methods which has been widely investigated [70]. It is based on the split-step Fourier method (SSFM) and the deterministic effects of the fiber channel which are described by the nonlinear Schrödinger equation (NLSE) are compensated. Drawbacks for this approach are the high computational complexity to solve the NLSE with inverse parameters ($-\alpha$, $-\beta_2$, and $-\gamma$) and the access to the complex signal over the whole bandwidth.

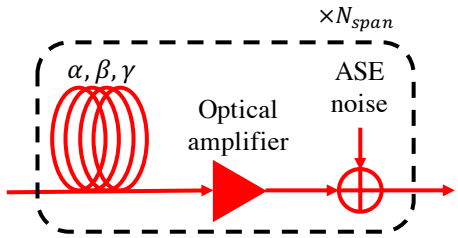

Figure 2.7: Multi-span fiber-optic channel model with inline optical amplification. The N_{span} indicates the number of spans. The fiber length in each span is L and the total propagation distance is $N_{span} \cdot L$.

2.3 Optical channel

In an optical communication system, the main medium in which the light is propagating to transfer the signal is the fiber link. The fiber consists of a cylindrical core surrounded by a ring-shaped cladding with a lower refractive index to confine and guide the light across the fiber. The main principle for light propagation inside the fiber is the total internal reflection at the boundary of the core and cladding. Depending on the core diameter, discrete set of modes can propagate inside the fiber. For single-mode fiber, the core diameter is usually 5-15μm and the cladding diameter is typically 125μm. To protect the bare fiber, a polymer coating with 250μm diameter is added to cover the cladding. In a single-mode fiber, the core and cladding are made of Silicon dioxide (SiO_2) and they are doped with other materials such as germanium dioxide to change the refractive index [71].

Other types of fibers are coupled or uncoupled multi-core, multi-mode, and few-mode fibers. Uncoupled multi-core fibers consist of several independent cores inside the cladding which are separated enough to minimize the coupling between the cores. These fibers can be viewed as parallel single-mode fibers, therefore, the conventional transceivers can be utilized. However, due to the separation between the cores, the cladding size might increase which affects the bending stress that they can tolerate. On the other hand, coupled multi-core fibers, provided denser packing of the cores inside the conventional cladding at the expense of coupling between the cores. Therefore, in the receiver, multiple-input and multiple-output (MIMO) signal processing is required. Multi-mode fibers are used in short-reach applications combined with vertical-

cavity surface-emitting lasers because of cost and energy efficiencies. Few-mode fibers are similar to multi-mode fibers, however, unlike multi-mode fiber, each mode is modulated with a different signal and they will require MIMO signal processing to compensate the mode coupling and recover the original signal in the receiver.

Below, some of the fiber impairments which have been considered in this thesis are introduced.

2.3.1 Fiber Losses

The optical power in fiber decreases as the light propagates across the length. This power loss or attenuation is denoted by α in the units of Np/km. In this unit, the power loss in fiber is described as

$$\frac{dP}{dz} = -\alpha P, \tag{2.11}$$

where P is the average optical power and z is the propagation distance. For a fiber with length L and input and output optical power of P_{in} and P_{out} the attenuation coefficient in dB/km is

$$\alpha_{[dB/km]} = -\frac{10}{L}\log_{10}\frac{P_{out}}{P_{in}} = -\frac{10}{L}\log_{10} e^{-\alpha L} = 4.343\alpha, \tag{2.12}$$

where in typical transmission fiber, $\alpha \approx 0.2$ dB/km.

One of the main reasons for fiber losses is the Rayleigh scattering. Randomly located molecules and local fluctuations in the fiber refractive index during manufacture causes the light to scatter in all directions. This intrinsic loss indicates the ultimate loss coefficient for fibers which is proportional to λ^{-4} where λ is the light wavelength. Another loss factor in fiber is the material absorption due to the small impurities such as OH ions [72, Chap. 1].

In a single-mode fiber, the wavelength regions are divided into six bands shown in Table 2.1. Among them, C and L bands are usually used for long-haul communication since their losses are minimized around 0.2 dB/km and amplifiers exist to compensate for the losses.

2.3.2 Chromatic dispersion

The refractive index of a fiber $n(\omega)$ is not constant over all wavelengths. This wavelength dependency results in different propagation speeds for different frequency components of the signal. In the frequency domain,

Band	Wavelength
O band	1260 nm - 1360 nm
E band	1360 nm - 1460 nm
S band	1460 nm - 1530 nm
C band	1530 nm - 1565 nm
L band	1565 nm - 1625 nm
U band	1625 nm - 1675 nm

Table 2.1: Optical communication wavelength bands

this corresponds to a phase shift which depends on the propagation distance. Therefore, in a dispersive fiber, the time-domain signal can broaden. This pulse broadening causes inter-symbol interference and limits the minimum pulse duration and the maximum data rate unless it is compensated.

In wave optics description of light, each fiber mode has a propagation constant $\beta(\omega)$. Taylor expanding β around the angular frequency ω_0 can provide dispersion parameters according to

$$\beta(\omega) = n(\omega)\frac{\omega}{c} = \beta_0 + \beta_1(\omega - \omega_0) + \frac{1}{2}\beta_2(\omega - \omega_0)^2 + \cdots, \tag{2.13}$$

where c is the speed of light in vacuum and

$$\beta_m = \left(\frac{\mathrm{d}^m\beta}{\mathrm{d}\omega^m}\right)_{\omega=\omega_0}, \quad m = 0, 1, 2, \cdots. \tag{2.14}$$

In equation (2.13), β_0 and β_1 are propagation constant and inverse group velocity, respectively, and β_2 is known as the *group-velocity dispersion* parameter and is given in the units of $\mathrm{ps}^2/\mathrm{km}$. The dispersion parameter D for the fiber is related to β_2 and is given by

$$D = -\frac{2\pi c}{\lambda^2}\beta_2, \tag{2.15}$$

and usually is reported in the units of ps/(km·nm). Typical values of D in standard fibers are in the range of 15-18 ps/(km·nm) near 1.55 μm.

2.3.3 Fiber Kerr nonlinearities

Due to the very small area of the fiber core, even small optical powers can create very high intensities which can change the properties of

fiber including the refractive index. Fiber refractive index n is not only a function of frequency ω but also the intensity of light that is propagating inside the fiber, i.e., $n = n(\omega, |E|^2)$ where E is the electric field amplitude. This relation causes a phase distortion on the light which depends on the signal power. This phase distortion can be generated from the signal itself (self-phase modulation) or the other signals in a different frequency, polarization, or propagation direction (cross-phase modulation).

2.3.4 Optical amplifiers

In modern long-haul optical communication systems, the optical signal undergoes optical amplification to compensate for fiber losses in the link. Optical amplifiers are a key enabling technology to pave the way for WDM systems. Because of their wide bandwidth, they are able to amplify many wavelength channels simultaneously, directly in the optical domain, which was not possible with the old optical-electrical-optical repeaters.

One of the most widely used optical amplifiers is the erbium-doped fiber amplifier which works based on stimulated emissions. The fiber inside these amplifiers is doped with the rare-earth element erbium so that it can absorb pump photons in one frequency (980 or 1480 nm) and emit photons at other frequencies. Usually, an external laser pumps the high energy light into the fiber amplifier to excite the erbium atoms. The input signal to the amplifier which can be in the wavelength range of 1530-1620 nm stimulates the excited atoms to emit photons at the same wavelength. This procedure amplifies the weak input signal and boosts its power.

However, this amplification is not noiseless. Because of the spontaneous emission of the excited erbium ions, usually, photons with a random phase, frequency, and polarization state rather than the input signal's are generated which reduces the signal quality at the output of the amplifier. These photons are incoherent with the input signal and will be amplified similarly to the input signal. Therefore, this additive noise is called *amplified spontaneous emission (ASE)* noise.

The power spectral density of the ASE noise is given by

$$\rho(f) = 2n_{sp}hf\left(G(f) - 1\right), \tag{2.16}$$

where $G(f)$ is optical gain at optical frequency f, n_{sp} is the spontaneous emission factor, h is the Planck's constant and the factor of 2 indicates

the two orthogonal polarization states. The power of the noise over the bandwidth $B = f_{max} - f_{min}$ is calculated as

$$P_{ASE} = \int_{f_{min}}^{f_{max}} \rho(f) \mathrm{d}f, \tag{2.17}$$

and if the bandwidth is narrow enough to consider a flat power spectral density around f_0, the noise power is

$$P_{ASE} \approx 2 n_{sp} h f_0 \left(G(f_0) - 1\right) B. \tag{2.18}$$

2.3.5 Additive white Gaussian noise channel

A simple approximation for the long-haul optical channels is the AWGN channel. The relation between the input $\mathbf{X}$ and output $\mathbf{Y}$ of this channel is given by

$$\mathbf{Y} = \mathbf{X} + \mathbf{Z} \tag{2.19}$$

where $\mathbf{X}$ and $\mathbf{Y}$ can denote multidimensional vectors. In fig. 2.1 and 2.4, the input $\mathbf{X}$ indicates data after constellation mapping block and output $\mathbf{Y}$ represent the data before decision block. The random vector $\mathbf{Z}$ models the noise and has a multidimensional Gaussian distribution expressed by

$$\mathbf{Z} \sim \mathcal{N}(\mathbf{0}, \mathbf{\Sigma}), \tag{2.20}$$

with a zero mean vector and the covariance matrix of $\mathbf{\Sigma} = \sigma^2 \mathbf{I}$ where σ^2 is the noise variance per dimension and $\mathbf{I}$ is the identity matrix [73].

The sources of Gaussian noise for the AWGN approximation of fiber channel are mainly the in-line optical amplifiers with the power given in (2.18).

2.3.6 Nonlinear Schrödinger equation

A detailed model of the lightwave propagation over the fiber link is given by solving the Maxwell's equations for a cylindrical waveguide. Under the assumptions of slowly varying envelope, weak higher order nonlinearities and dispersion, instantaneous nonlinear response and low fiber losses, the final differential equation is known as the NLSE [72] described by

$$\frac{\partial E}{\partial z} = -\frac{\alpha}{2} E - i \frac{\beta_2}{2} \frac{\partial^2 E}{\partial t^2} + i \gamma |E|^2 E, \tag{2.21}$$

where $E(z,t)$ is light pulse envelope at distance z and time t which is measured in a reference frame moving with the pulse at the group velocity $\nu_g = 1/\beta_1$, α is the loss, β_2 is the group velocity dispersion, and γ is the nonlinear coefficient defined as $\gamma = 2\pi n_2/(\lambda A_{\text{eff}})$ with nonlinear Kerr parameter n_2 and the effective mode area A_{eff}. The A_{eff} depends on the mode transverse distribution which is related to the core radius and core-cladding index difference. In fig. 2.7, $E(0,t)$ and $E(L,t)$ are the input and output of the fiber channel, respectively, where L is the fiber length.

For a dual polarization signal, the NLSE can be extended to the Manakov equations [74, 75]

$$\frac{\partial E_x}{\partial z} = -\frac{\alpha}{2}E_x - i\frac{\beta_2}{2}\frac{\partial^2 E_x}{\partial t^2} + i\frac{8}{9}(|E_x|^2 + |E_y|^2)E_x, \tag{2.22}$$

$$\frac{\partial E_y}{\partial z} = -\frac{\alpha}{2}E_y - i\frac{\beta_2}{2}\frac{\partial^2 E_y}{\partial t^2} + i\frac{8}{9}(|E_x|^2 + |E_y|^2)E_y, \tag{2.23}$$

where $E_x(z,t)$ and $E_y(z,t)$ are the pulse envelopes for two orthogonal polarizations. The factor $8/9$ comes from the averaging due to the random birefringence along the fiber [74].

In order to solve the NLSE or Manakov equations, the SSFM is usually used [72]. This method separates the linear and nonlinear operations in the main partial differential equation and solves them separately in frequency and time domains, respectively, with small step sizes to control the error caused by this splitting. However, using a small step size increases the computational complexity and can make this method very time-consuming [76].

To reduce the complexity of SSFM, many efforts have been made to approximate the nonlinear fiber channel. Among them, the Gaussian noise (GN) model has been proposed and widely used because of its low complexity [77]. This model assumes that the interaction of fiber nonlinearities and chromatic dispersion results in an additive Gaussian noise for the received signal. This model requires a long-haul link without inline dispersion compensation. During propagation, chromatic dispersion spreads the signal and due to nonlinearity, the signal interacts with itself continuously. According to the central limit theorem, the summation of many independent random variables results in a random variable with a Gaussian distribution which motivated (2.19). It has been shown that the power spectral density of this noise depends on the transmitted signal power via a cubic relationship [78]. Finally, in the receiver, the quality

of the signal is reduced due to both the in-line amplifier noise and the additive Gaussian noise of the dispersion and nonlinearity interaction.

CHAPTER 3

Modulation formats

In early optical communication networks, intensity-based modulation formats were dominant because of the low-complexity transmitter and receiver configurations [79]. These noncoherent formats are usually referred to as intensity modulation with direct detection (IM/DD) since they do not require a separate phase reference to be detected and the variation of the light intensity is captured by a photo-detector. Modulation formats that fall in this category are on-off keying and pulse-amplitude modulations. Together with WDM technology, noncoherent formats were able to provide sufficient performance in terms of reach and rate up until 2010. However, by increasing the demands, the SE and sensitivity of these modulation formats became a limiting factor for further improvements.

In order to overcome these limitations, coherent detection in the 4-dimensional space of light has been developed to both increase the SE by multi-level modulation formats [80] and improve the sensitivity by designing modulation formats in multidimensional space [81]. Modulating amplitude, phase, polarization, frequency, time, and spatial mode of the optical signal provide more degrees of freedom to achieve higher order modulation formats with more signal levels to increase the SE thus transmitting more bits in each channel use [82, 83]. Today, coherent detection combined with DSP is able to compensate for most of the link impairments digitally rather than using physical hardware [84]. This

fact has reduced the hardware implementation complexity of coherent detection significantly and has made it a preferred solution for long-haul communication links compared to IM/DD approaches which are used in short-haul and low-cost links.

Moreover, because of coherent detection which provides access to higher dimensions of optical signal, modulation format optimization has also gained attention to improve the modulation sensitivity and designing constellations which are more robust to link impairments including the transmitter, receiver and the fiber channel [85, 86].

In this chapter, we introduce the basic definitions for modulation format including the multidimensional representation. Then, the most common metrics used to compare modulation formats are presented.

3.1 Basic definitions

In optical communication links, the optical field amplitude at the output of the transmitter into the fiber channel can be modeled as

$$\mathbf{E}(t) = \sum_i \sqrt{P_{s,i}} e^{j(\omega_{s,i}t+\phi_{s,i})} \cdot \mathbf{s}_i(t), \tag{3.1}$$

where $\mathbf{s}(t)$ is the normalized complex envelope with a time dependent amplitude and phase over the two polarization states. The P_s, ω_s, and ϕ_s indicate the power, frequency, and phase of the optical carrier. Index i shows the number of different frequency channels that are propagating together in the fiber as shown in fig. 3.1. In (3.1), the degrees of freedom which can be used to modulate the carrier in a single mode fiber are frequency and complex envelope which includes the polarization states. In each frequency, the complex envelope is described by a complex vector

$$\mathbf{s}(t) = \sum_k \mathbf{c}_k \cdot h(t - kT), \quad \mathbf{c}_k = \begin{bmatrix} I_x^k + jQ_x^k \\ I_y^k + jQ_y^k \end{bmatrix}, \tag{3.2}$$

where I and Q are real numbers indicating the IQ components of the electrical field, respectively. The x and y stand for the two orthogonal polarization states. Also, k indicates the time slot in which the data is transmitted and $h(t)$ is the pulse shaping function with duration T and unit average energy.

In each wavelength and polarization components, the corresponding complex envelope can be geometrically represented in the Cartesian coordinate system where one axis is used to present the real part of the complex number and the other axis shows the imaginary part.

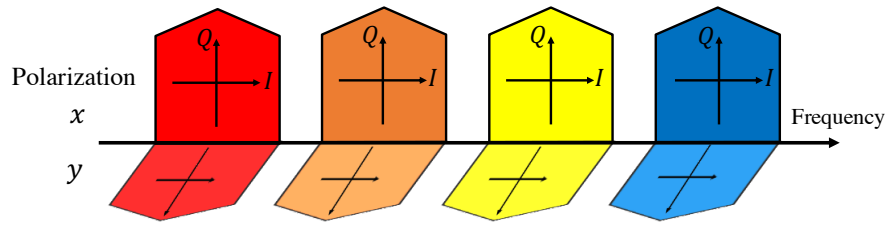

Figure 3.1: Multidimensional transmission in single mode fiber. Different colors indicate different wavelengths. At each wavelength, two orthogonal polarizations and IQ components are used.

Alternatively, the combinations of all available carrier frequencies, IQ components, polarizations, spatial modes, and time slots can be considered as orthogonal dimensions. In this approach, the transmitted signal is represented as

$$\mathbf{E}(t) = \sum_{k} \sum_{n=0}^{N-1} c_{k,n} \Phi_n(t - kT), \tag{3.3}$$

where the real vector $\mathbf{c}_k = [c_{k,0}, c_{k,1}, \cdots, c_{k,N-1}]$ is the kth transmitted symbol, N is the dimensionality, and $\{\Phi_n(t)\}$ is the set of all possible combinations of dimensions which are related to carrier frequency, time slot, IQ components, spatial mode, and polarization. The combination of these dimensions generates a set where its elements are orthogonal to each other, i.e.,

$$\frac{1}{T} \int_0^T \Phi_n(t) \Phi_m(t) \mathrm{d}t = \delta_{n,m}, \tag{3.4}$$

where δ is Kronecker delta function.

The vector $\mathbf{c}_k$ is chosen from a set of points called *constellation* $\mathcal{C} = \{\mathbf{c}_0, \mathbf{c}_1, \cdots, \mathbf{c}_{M-1}\}$ with M symbols. The average energy of the constellation is given by

$$E_s = \sum_{i=0}^{M-1} p(\mathbf{c}_i) \left\| \mathbf{c}_i \right\|^2, \tag{3.5}$$

where $p(\mathbf{c}_i)$ is the probability of symbol $\mathbf{c}_i$, $\left\| \mathbf{c}_i \right\|^2$ is the symbol energy and $\|\cdot\|$ is used to calculate the Euclidean norm of a multidimensional vector. For a constellation with uniform probability distribution, (3.5) is simplified to $E_s = (1/M) \sum_{i=0}^{M-1} \left\| \mathbf{c}_i \right\|^2$.

The constellation entropy is defined as

$$\mathbb{H}(\mathcal{C}) = -\sum_{i=0}^{M-1} p(\mathbf{c}_i) \log_2 p(\mathbf{c}_i), \tag{3.6}$$

which is the average number of bits required to represent each symbol. For constellations with uniform probability distribution, $\mathbb{H}(\mathcal{C}) = \log_2 M$ and the average energy per bit is $E_b = E_s / \log_2 M$.

Another property of the constellation is the Euclidean distance between the constellation points $d_{ij} = \|\mathbf{c}_i - \mathbf{c}_j\|$ where its minimum value d_{min} gives the performance of the constellation at high SNR.

The geometrical representation of the the transmitted information using multidimensional vectors bring us the possibility of looking into denser packings which-at the same d_{min}-provide a reduced constellation energy E_s. This topic in literature is known as *sphere packing* [87]. Investigating the performance of these modulation formats is the main contribution of this thesis which will be discussed in the following chapter.

3.2 Figures of Merit

In this section, we introduce parameters which can be used to compare the properties of modulation formats or their performance over a channel.

3.2.1 Spectral efficiency

For a constellation $\mathcal{C}$ with M symbols in N dimensions and uniform probability distribution, the SE is defined as

$$\beta = \frac{\log_2 M}{N/2}, \tag{3.7}$$

and has the unit of bits per symbol per dimension pair [88]. This parameter measures the SE for an uncoded transmission system. In fiber-optic communication, usually, the polarization of light is considered as a pair of dimensions because each polarization can support two IQ components.

Another definition for SE is based on the transmitted rate over a specific bandwidth. In this case, the unit is defined as bits per second per Hertz.

3.2.2 Symbol and bit error rate

The symbol error rate (SER) and bit error rate (BER) are metrics to show the performance of the transmission over the channels and they simply show the number of errors in transmitted symbols or bits that have happened during the transmission. For equiprobable constellations with maximum likelihood (ML) estimation, using pairwise error probability and the so-called union bound [48, Chap. 4], the SER is bounded by

$$\mathrm{SER} \leq \frac{1}{M} \sum_{i=0}^{M-1} \sum_{j \neq i} \frac{1}{2} \mathrm{erfc}\left(\frac{d_{ij}}{2\sqrt{N_0}} \right), \tag{3.8}$$

where d_{ij} is the Euclidean distance between constellation points $\mathbf{c}_i$ and $\mathbf{c}_j$, $\mathrm{erfc}(x) = (2/\sqrt{\pi}) \int_x^\infty \exp(-t^2) dt$ is the complementary error function and $N_0/2$ is the variance of the Gaussian noise in each dimension. For high SNR, the terms with $d_{ij} = d_{min}$ dominate and the SER is bounded by

$$\mathrm{SER} \lessapprox \frac{\bar{\tau}}{2} \mathrm{erfc}\left(\frac{d_{min}}{2\sqrt{N_0}} \right), \tag{3.9}$$

which $\lessapprox$ means an approximate upper bound that approaches the true value as N_0 goes to zero. Here, $\bar{\tau} = (1/M) \sum_{i=0}^{M-1} \tau_i$, where τ_i is the number of neighbours at the minimum distance from symbol $\mathbf{c}_i$.

The BER depends on the bit labeling of the symbols as well. There are various ways to assign bit labels to constellation points. In this thesis, the focus is on the natural binary and Gray labeling for QAM formats. Two examples are shown in fig. 3.2 where the top black color represents Gray labeling and the bottom red color shows the natural binary. The SER and BER of QAM formats over the AWGN channel are shown in fig. 3.3.

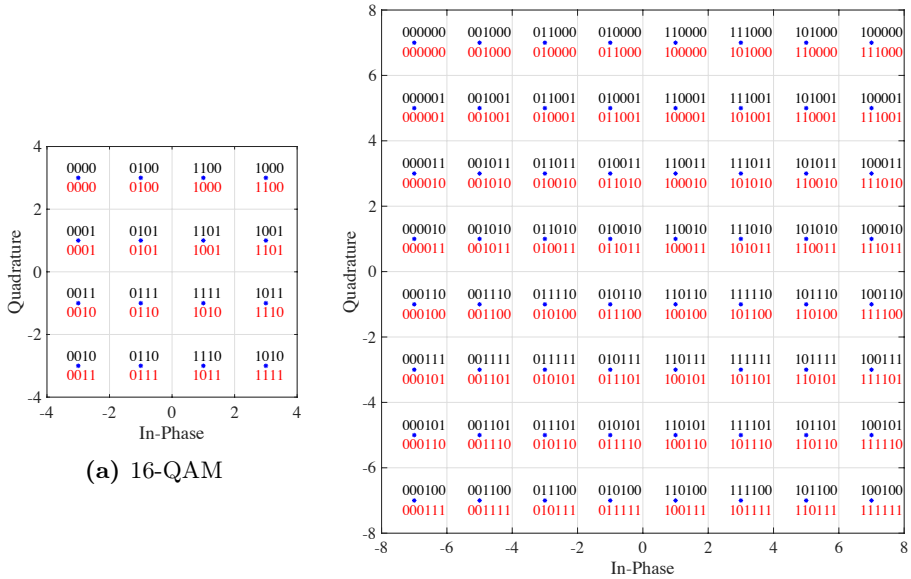

(a) 16-QAM

(b) 64-QAM

Figure 3.2: The natural and Gray labeling for QAM constellations. The top black color indicates the Gray labeling and the bottom red color shows the natural binary labeling.

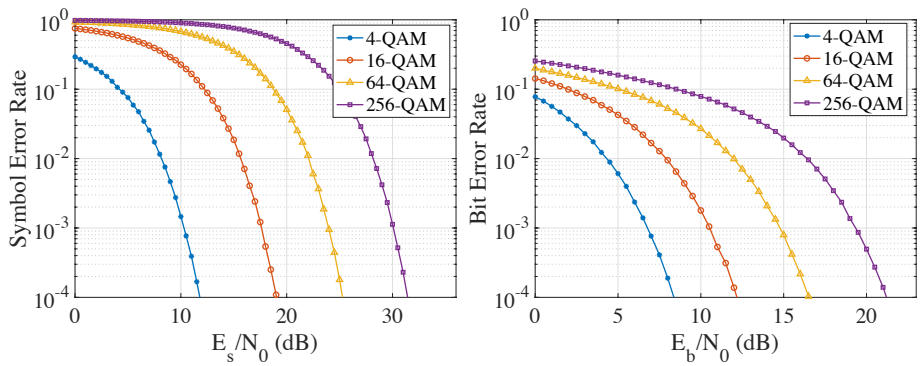

(a) SER

(b) BER

Figure 3.3: The SER and uncoded BER performance of QAM formats with uniform probability distribution over the AWGN channel. The BER is for Gray mapped constellations.

3.2.3 Asymptotic power efficiency

For the AWGN channel, at high SNRs, the SER is approximated by the union bound in (3.8) which includes the error probability terms that are based on the minimum Euclidean distance transitions (d_{min}), i.e., $\mathrm{erfc}(d_{min}/(2\sqrt{N_0}))$. Therefore, the SER is a monotonically decreasing function of

$$\frac{d_{min}^2}{4N_0} = \frac{P}{R_b N_0}\gamma = \frac{E_b}{N_0}\gamma, \tag{3.10}$$

where $\gamma = d_{min}^2/(4E_b)$ is defined as the asymptotic power efficiency (APE). This parameter depends on the constellation geometry. For binary phase-shift keying (BPSK), QPSK and dual polarization QPSK modulation formats, the γ value is equal to 0 dB. The sensitivity penalty is also defined as $1/\gamma$ and it shows the performance penalty compared to BPSK, QPSK and dual polarization QPSK for high SNR [45]. The relation between SE and APE is shown for QAM and 4-dimensional set partitioning (SP)-QAM in fig. 3.4. The SP-QAM is generated from the 4-dimensional QAM by selecting every second point. The analytical expression for SE and APE for QAM and SP-QAM are [89]

$$\text{QAM}: \quad \gamma = \frac{3SE}{2(2^{SE}-1)}, \quad SE/2 \text{ is integer} \tag{3.11}$$

$$\text{SP-QAM}: \quad \gamma = \begin{cases} \frac{3SE}{2^{(SE+0.5)}-1}, & SE+0.5 \text{ is even} \\ \frac{3SE}{2^{(SE+0.5)}-0.5}, & SE+0.5 \text{ is odd} \end{cases} \tag{3.12}$$

3.2.4 Mutual information

Since around 2010, soft-decision (SD) forward error correction (FEC) schemes have become popular in the optical communication society because of their improved performance [90]. This improvement comes at the expense of a higher complexity with respect to hard-decision (HD) FEC. In contrast to the HD FEC decoder which works with the estimated symbols or bits, SD FEC decoder depends on the soft information such as the likelihood of the received information. Therefore, for the SD FEC decoder, there is not a direct relation between pre-FEC and post-FEC BERs [91, 92]. A better metric for SD FEC is the generalized mutual information (GMI).

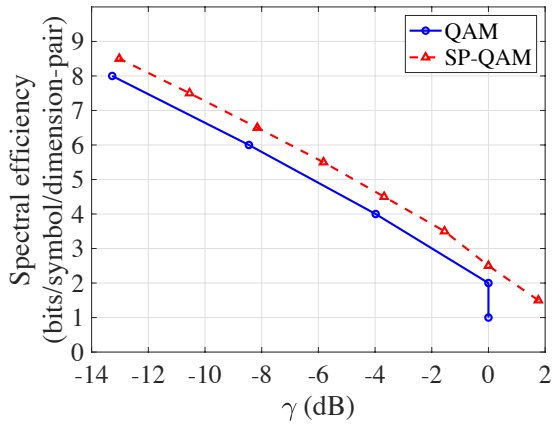

Figure 3.4: The SE vs APE (γ) for QAM formats and SP-QAM.

Assuming a discrete memoryless channel with multidimensional input vector $\mathbf{X}$ and output $\mathbf{Y}$, and channel transition probability density of $p_{\mathbf{Y}|\mathbf{X}}(\mathbf{y}|\mathbf{x})$, the mutual information (MI) is calculated as

$$\begin{aligned} MI = \mathbb{I}(\mathbf{X};\mathbf{Y}) &= \mathbb{E}\left[\log_2 \frac{p_{\mathbf{Y}|\mathbf{X}}(\mathbf{Y}|\mathbf{X})}{p_{\mathbf{Y}}(\mathbf{Y})}\right] = \mathbb{E}\left[\log_2 \frac{p_{\mathbf{X},\mathbf{Y}}(\mathbf{X},\mathbf{Y})}{p_{\mathbf{X}}(\mathbf{X})p_{\mathbf{Y}}(\mathbf{Y})}\right] \\ &= \int_{\mathbb{R}^N}\int_{\mathbb{R}^N} p_{\mathbf{X},\mathbf{Y}}(\mathbf{x},\mathbf{y}) \log_2 \frac{p_{\mathbf{X},\mathbf{Y}}(\mathbf{x},\mathbf{y})}{p_{\mathbf{X}}(\mathbf{x})p_{\mathbf{Y}}(\mathbf{y})} d\mathbf{x}d\mathbf{y} \\ &= \int_{\mathbb{R}^N}\int_{\mathbb{R}^N} p_{\mathbf{X}}(\mathbf{x})p_{\mathbf{Y}|\mathbf{X}}(\mathbf{y}|\mathbf{x}) \log_2 \frac{p_{\mathbf{Y}|\mathbf{X}}(\mathbf{y}|\mathbf{x})}{p_{\mathbf{Y}}(\mathbf{y})} d\mathbf{x}d\mathbf{y} \\ &= \sum_{\mathbf{x}\in\mathcal{C}} p_{\mathbf{X}}(\mathbf{x}) \int_{\mathbb{R}^N} p_{\mathbf{Y}|\mathbf{X}}(\mathbf{y}|\mathbf{x}) \log_2 \frac{p_{\mathbf{Y}|\mathbf{X}}(\mathbf{y}|\mathbf{x})}{p_{\mathbf{Y}}(\mathbf{y})} d\mathbf{y}, \end{aligned} \tag{3.13}$$

where the $p_{\mathbf{X}}$ and $p_{\mathbf{Y}}$ are the marginal distributions of the input and output and $p_{\mathbf{X},\mathbf{Y}}$ is the joint distribution. Since the input constellation points are discrete, the continuous integral over the input can be replaced with a discrete summation in the last step.

Instead of calculating the multidimensional integrals in (3.13), one can use the Monte-Carlo method to approximate the MI as

$$MI \approx \frac{1}{K}\sum_{i=1}^{K} \log_2 \frac{p_{\mathbf{Y}|\mathbf{X}}(\mathbf{y}_i|\mathbf{x}_i)}{p_{\mathbf{Y}}(\mathbf{y}_i)}, \tag{3.14}$$

where K is the number of random samples over the channel.

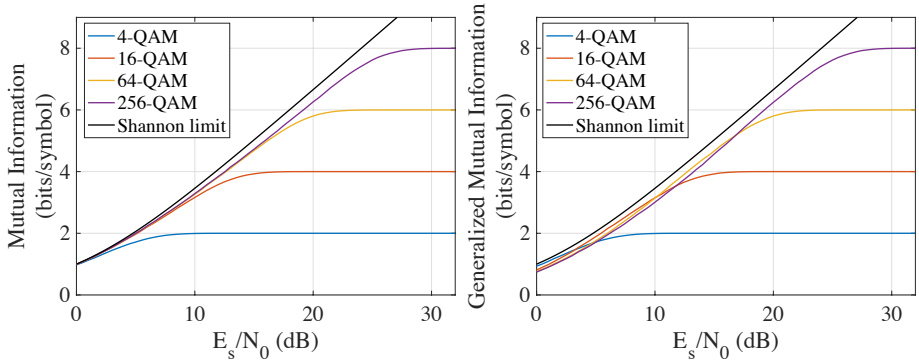

(a) MI **(b)** GMI

Figure 3.5: The MI and GMI performance of QAM formats over the AWGN channel. The Shannon limit is defined as $\log_2(1 + E_s/N_0)$.

Similar to the BER, the GMI depends on the bit labeling of the constellation points. The GMI is defined as an achievable information rate for a bit-wise decoder. For a channel with input $\mathbf{X}$, symbol label of $b_0 b_1 \cdots b_{m-1}$, and output $\mathbf{Y}$, the mutual information can be expanded as

$$\begin{aligned}\mathbb{I}(\mathbf{X};\mathbf{Y}) &= \mathbb{I}(b_0, b_1, \cdots, b_{m-1}; \mathbf{Y}) \\ &= \mathbb{I}(b_0;\mathbf{Y}) + \mathbb{I}(b_1;\mathbf{Y}|b_0) + \cdots + \mathbb{I}(b_{m-1};\mathbf{Y}|b_0, b_1, \cdots, b_{m-2}).\end{aligned} \tag{3.15}$$

In this equation, each term provides a binary-input channel and a binary code can be applied for error correction. This is referred as a multi-stage decoder where lower-index bit levels provide side information for decoding of higher level bits [93]. However, this scheme comes at expense of latency, memory to store channel output, and an individual code for each sub-channel. If we neglect the side conditioning, the result will be known as the GMI

$$GMI = \mathbb{I}(b_0;\mathbf{Y}) + \mathbb{I}(b_1;\mathbf{Y}) + \cdots + \mathbb{I}(b_{m-1};\mathbf{Y}) = \sum_{i=0}^{m-1} \mathbb{I}(b_i;\mathbf{Y}). \tag{3.16}$$

A more general defenition for GMI is given in equation (12) in [92].

Generally, the MI is greater than the GMI and the rate loss is due to the suboptimal bit-wise decoder. For Gray-labeling, this rate reduction is shown to be very small [94]. The MI and GMI for QAM formats are shown in fig. 3.5 over the AWGN channel.

Normalizing the GMI with the number of transmitted bits per symbol results in the normalized generalized mutual information (NGMI), i.e.,

$$NGMI = \frac{1}{m} GMI = \frac{1}{m} \sum_{i=0}^{m-1} \mathbb{I}(b_i; \mathbf{Y}). \tag{3.17}$$

For a nonuniform source, the NGMI is defined as [95]

$$NGMI = 1 - \frac{\mathbb{H}(\mathbf{X}) - GMI}{\log_2 M}. \tag{3.18}$$

The NGMI can be used to predict the post-FEC BER in SD systems without implementing the encoder and decoder. Such predictions have been shown in [91] for different coding schemes and code rates.

CHAPTER 4

Constellation Shaping

The recent increasing demands for higher data rates in communication systems have forced the system designers to operate closer to channel capacity than before [96]. To achieve this goal, the source is optimized to maximize the mutual information between the input and output of the channel [97]. In information theory, this optimization is called *constellation shaping* and it is defined as finding energy-efficient methods for the communication system to improve the performance compared with the conventional QAM formats [98]. The horizontal gaps in the MI and GMI plots shown in fig. 3.5 are the shaping gains that can be achieved compared with QAM formats.

In a simple approximation of the fiber-optic communication link showed in chapter 2, the optical fiber channel is assumed as an AWGN channel where the main source of noise is the amplified spontaneous emission noise from the optical amplifiers in the link. It has been shown that for an AWGN channel, the capacity achieving source distribution is the Gaussian probability [99]. Therefore, the proposed constellation distribution should approximate the Gaussian distribution for the transmitted symbols.

Two main classification of constellation shaping methods are PS and GS. The purpose of PS is to change the occurrence probability of the constellation points with respect to a uniform probability distribution. On the other hand, GS is focused on the geometric representation of the

constellation in the Euclidean space and it tries to optimize the position of the constellation points to mimic a hyperspherical boundary. As shown in fig. 3.5, compared with QAM formats, the maximum shaping gain that can be achieved by constellation shaping is 1.53 dB over the AWGN channel with a hyperspherical boundary as the dimensionality goes to infinity [95].

In this chapter, the basic definition about these methods are introduced followed by possible practical implementation in optical fiber communication systems.

4.1 Probabilistic Shaping

The capacity of a communication channel is achieved by optimizing the probability distribution of the source [100], i.e.,

$$C = \max_{p_{\mathbf{X}}} \mathbb{I}(\mathbf{X}; \mathbf{Y}), \tag{4.1}$$

where C is the channel capacity with the optimum $p_{\mathbf{X}}$ and $\mathbb{I}$ shows the mutual information. However, finding the optimum distribution is not always possible and sometimes the channel itself is mathematically complicated, e.g., nonlinear optical fiber channel [28].

The PS is a method to employ source distributions other than the uniform distribution to increase the information rate transmission under the constraint of limited average power [33]. In an AWGN channel, the input Gaussian distribution maximizes the mutual information between the input and output of the channel and results in the famous Shannon capacity formula [26]. Usually, the source is considered with discrete symbols or messages. Therefore, a discrete Gaussian-like distribution, namely the Maxwell-Boltzmann (MB) distribution, should be used to optimize the MI in the AWGN channel [101].

Under no constraints, the probability distribution that maximizes the source entropy ($\mathbb{H}(\mathbf{X})$) is the uniform probability distribution. If the source is limited to have a maximum average power ($\mathbb{E}(\|\mathbf{X}\|^2) \leq P$), the distribution that maximizes the source entropy is the MB distribution. The probability of generating each symbol at the transmitter is given by

$$p_{\mathbf{X}}(\mathbf{x}) = \frac{1}{\sum_{\mathbf{x}' \in \mathcal{C}} \exp(-\nu \left\|\mathbf{x}'\right\|^2)} \exp(-\nu \|\mathbf{x}\|^2), \tag{4.2}$$

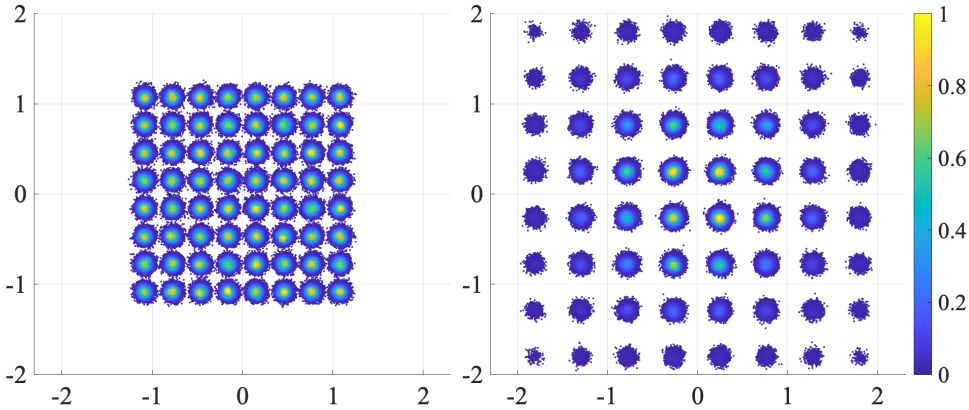

(a) $\nu = 0$ **(b)** $\nu = 2.69$

Figure 4.1: Uniform and probabilistically shaped 64-QAM at the same SNR with 6 and 5 bits/symbol source entropy, respectively. The color bar shows the normalized probability of occurrence.

where ν is the shaping factor. For $\nu = 0$, the probability distribution becomes uniform and for $\nu > 0$, the constellation points will have a nonuniform probability. Increasing ν causes the inner points of the constellation to have higher probability than the outer constellation points as shown in fig. 4.1.

The MI between the input and output of the channel depends on the shaping factor ν and the SNR. In fact, it has been shown that for every SNR, there is an optimum ν which maximizes the MI over the AWGN channel [102]. Choosing the optimized shaping factor at each SNR will change the source entropy at the corresponding SNR. On the other hand, setting the shaping factor to a fixed value for all SNRs will result in a source with a fixed source entropy. The effect of applying a constant shaping factor or optimizing the shaping factor at each SNR is shown in fig. 4.2.

Different schemes have been suggested for the implementation of PS, but the one which has got significant attention in the optical communications community is the probabilistic amplitude shaping (PAS). The PAS applies coding and shaping in an independent structure with separate optimizations which reduces the problem of burst errors and shaping distortion which are presented in other realizations of PS [95]. In fig. 4.3, the block diagram of a common realization of a PAS transmitter and receiver is presented [103]. In the transmitter, the splitter divides the

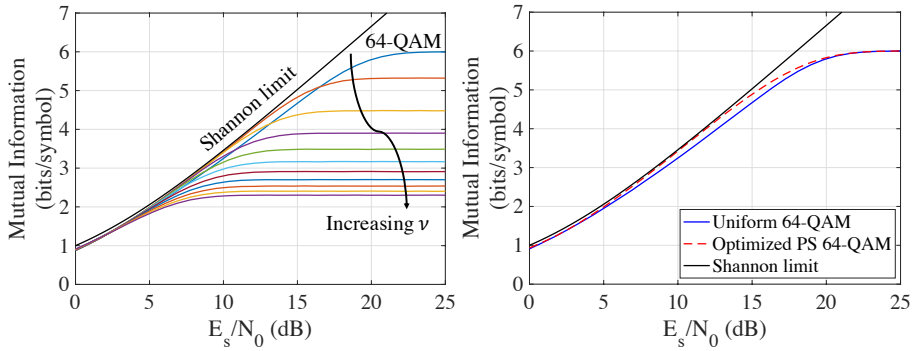

(a) Fixed ν for each line

(b) Optimized ν at each SNR

Figure 4.2: Effect of changing the shaping factor ν on the MI of the transmitted and received symbols.

input bit stream into two branches. The top branch is fed into the distribution matcher which generates a group of amplitudes based on the desired probability distribution, e.g., Maxwell-Boltzmann distribution. This amplitudes are labeled in the Gray mapping block and generate another stream of bits. Together with the bottom branch, these bits are encoded by a systematic FEC encoder. At this stage, the number of bits should be equal to the number of amplitudes after the distribution matcher. After the FEC, the bits $\{b_i\}$ are used to form the sign bits using $(-1)^{b_i}$ mapping and generate one dimension of the constellation. With the same procedure in the other dimension, the probabilistically shaped QAM can be generated. In the receiver, the received dimension is decoded to generated the desired reliability metric for bits which is fed into to the FEC decoder. Then, the inverse of shaping is applied to recover an estimate for the transmitted bits.

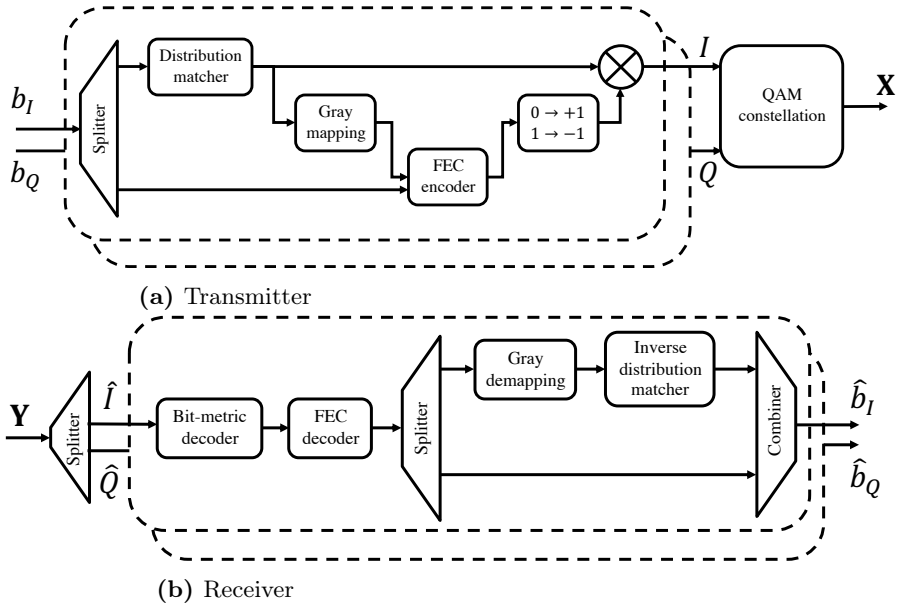

Figure 4.3: The transmitter and receiver block diagram for the PAS scheme with independent IQ components [103].

4.2 Geometric Shaping

Similar to PS, GS is also used to mimic the Gaussian distribution by another approach. Rather than changing the probability of generating each constellation point, for GS the probability of the constellation points is uniform, however, to shape the constellation, the position of constellation points in the Euclidean space is changed compared with the conventional cubic structures (QAM formats) which are widely used in communication systems. The geometrically shaped constellation results in a Gaussian distribution in the projection of the constellation to lower dimensions, e.g., one-dimensional projection.

Usually GS has been done by optimizing the position of the constellation points in an irregular structure in two-dimensional space to optimize a metric such as GMI [104]. This approach becomes complicated as the number of constellation points or dimensionality increases, and because of the irregular and spherically distributed points, a look-up table is required to store the coordinates of the symbols.

Recently, machine learning methods have also gained a lot of attention to substitute the whole transmitter and receiver design by neural

networks [105–107]. In this way, constellations can be designed using an end-to-end learning. Moreover, the GS and PS have been combined together using neural networks to design constellations which perform closer to the Shannon capacity limits [108].

Another method which is in focus for this thesis is multidimensional geometric shaping [109]. In this approach, instead of looking into irregular structures in Euclidean space, we use multidimensional lattice structures which provide regular point set in the multidimensional space [87]. Lattices in multidimensional space can provide both shaping and coding gain with respect to cubic constellation with cubic boundaries. The shaping gain is achieved by a boundary which is closer to a hypersphere in the multidimensional space and coding gain comes from the denser packing of the points. Below, some of the known lattices are introduced.

- Cubic (integer) lattice
  This lattice is the famous structure which the conventional QAM format is extracted with a cubic boundary. Generally, it is described as
  $$\mathbb{Z}^N = \{(x_0, x_1, \cdots, x_{N-1}) \mid x_i \in \mathbb{Z}\}, \tag{4.3}$$
  where $\mathbb{Z}$ is the set of integer numbers.

- Hexagonal lattice
  This lattice is famous in 2 and 3 dimensions since it provides the optimum lattice packing in these dimensions. It can be described by
  $$A_N = \left\{(x_0, x_1, \cdots, x_N) \mid x_i \in \mathbb{Z}, \sum_i x_i = 0\right\}. \tag{4.4}$$

- Checkerboard lattice
  A chess board can be considered as an example for this lattice in 2 dimensions. This lattice is described as
  $$D_N = \left\{(x_0, x_1, \cdots, x_{N-1}) \mid x_i \in \mathbb{Z}, \ \sum_i x_i \text{ is even}\right\}. \tag{4.5}$$

- Gosset lattice
  This lattice is defined in 8-dimensional space and it is described as
  $$E_8 = \left\{\mathbf{x} = (x_0, x_1, \cdots, x_7) \mid \mathbf{x} \in \mathbb{Z}^8 \bigcup (\mathbb{Z} + \frac{\mathbf{1}}{\mathbf{2}})^8, \ \sum_{i=0}^{7} x_i \equiv 0 \pmod 2\right\}. \tag{4.6}$$

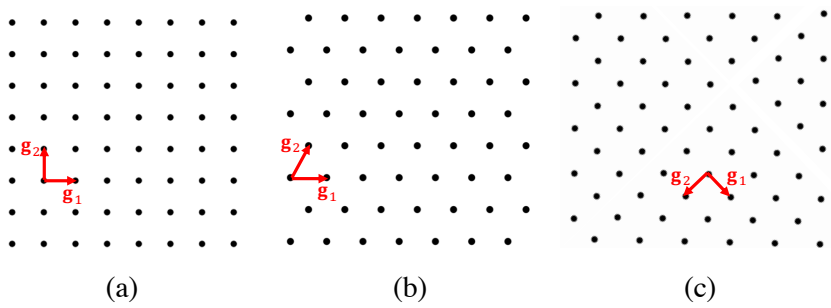

Figure 4.4: Example of lattices in 2 dimensions, (a) cubic, (b) hexagonal, and (c) checkerboard lattice. The basis vectors are shown in red arrows.

- Leech lattice
  This lattice is defined in 24-dimensional space and it provides optimum lattice packing in 24 dimensions. There are many descriptions for this lattice and they can be found in [87, Chap. 24].

An example of the first three lattices in 2 dimensions are shown in fig. 4.4. Beside these descriptions, the points in a lattice can be easily generated using its *generator matrix* $\mathbf{G}$. The generator matrix consists of linearly independent column vectors called basis vectors $[\mathbf{g}_0, \mathbf{g}_1, \cdots, \mathbf{g}_{N-1}]$. Therefore, a lattice can be generated by

$$\Lambda = \{z_0\mathbf{g}_0 + z_1\mathbf{g}_1 + \cdots + z_{N-1}\mathbf{g}_{N-1} \mid z_i \in \mathbb{Z}\} = \{\mathbf{G}\mathbf{z} \mid \mathbf{z} \in \mathbb{Z}^N\}. \quad (4.7)$$

As it is defined in (4.7), lattices are infinite sets of points. In order to use them as a modulation format, a finite number of points inside a specific boundary should be selected. For instance, QAM formats are the points selected from $\mathbb{Z}^2$ within a square boundary. Other types of boundaries rather than the cubic boundary are circular boundary and the scaled Voronoi region. Constellation mapping and demapping using circular boundaries are difficult and usually require look-up tables to store the constellation points. Due to complexity and gain factors, the focus of our work has been on the scaled Voronoi region. The Voronoi region of a lattice point is defined as the set of all points in $\mathbb{R}^N$ which are closer to that point than any other lattice points. This region is closer to a hypersphere boundary compared to a hypercubic boundary, and therefore it can provide shaping gain.

Table 4.1: Shaping and coding gains of multidimensional lattices [110], [47, Chap. 5]

Lattice	$\mathbb{Z}^N$	A_2	D_4	E_8	Λ_{24}
γ_c (dB)	0	0.62	1.51	3.01	6.02
γ_s (dB)	0	0.17	0.37	0.65	1.03

The APE of a constellation is related to two important gains which are separable at high SEs. For lattices, these gains are called shaping and coding gains and can be defined as [47]

$$\gamma_s(\mathcal{R}) = \frac{1}{12}\frac{N \cdot V(\mathcal{R})^{1+2/N}}{\int_{\mathcal{R}} \|\mathbf{r}\|^2 \, d\mathbf{r}} \tag{4.8}$$

$$\gamma_c(\Lambda) = \frac{d_{min}^2}{V(\Lambda)^{2/N}}, \tag{4.9}$$

which $V(\mathcal{R})$ stands for the volume of the shaping region and $V(\Lambda)$ is the fundamental lattice volume which is equal to the Voronoi region of any lattice points. The shaping and coding gain of various lattices are given in Table 4.1

The encoding of bits to the constellation points inside the scaled Voronoi region and decoding from them have been discussed in details in [Paper A] and [111].

After generating the N-dimensional constellation points, they need to be mapped to the optical signal. There are multiples ways to do this and an example has been shown in fig. 4.5. In this example, polarization, IQ, and frequency have been used as the dimensions. Other degrees of freedom, e.g., time slots and spatial modes, can also be used to increase the number of dimensions. The performance may depend on which dimensions are selected. Since, at each wavelength, the optical signal can carry a 4-dimensional vector including two polarization and two IQ components, an N-dimensional constellation point needs to be transmitted over $N/4$ different wavelengths. Then, these wavelengths are multiplexed together to form a WDM signal. In the receiver, these wavelengths are detected and processed separately and the 4-dimensional outputs are combined to form the received N-dimensional vector which is decoded by a lattice decoder [Paper A] to find the estimated bits.

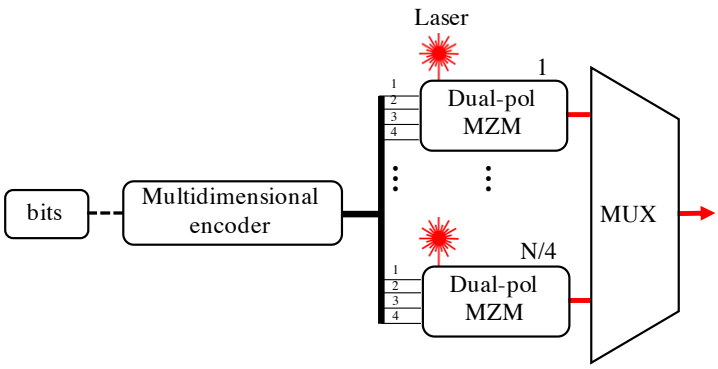

(a) Transmitter

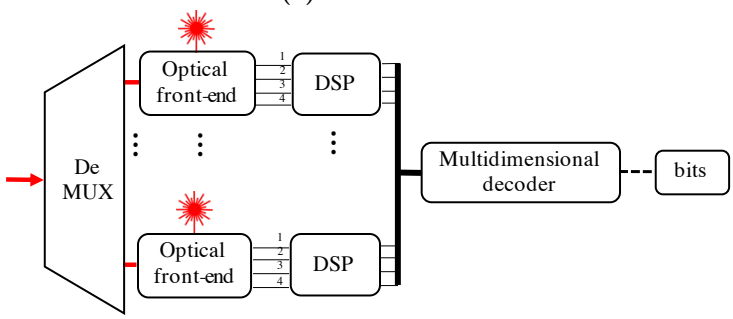

(b) Receiver

Figure 4.5: An example of multidimensional geometric shaping transmitter and receiver over a single-mode fiber.

CHAPTER 5

Future outlook

In this chapter, some future related topics to this thesis are discussed.

Multidimensional geometric shaping can be further investigated in scenarios including:

Comparison of different dimensions realization
In this thesis, realization of high-dimensional constellation over frequency, polarization, and IQ components were considered. Including other dimensions, e.g., space and time, could provide more degrees of freedom and different noise statistics which results in a different performance.

Performance with both the transmitter and channel impairments
In this thesis, only the optical fiber channel impairments has been considered for the geometrically shaped constellations. Because of the non-ideal components of the transmitter in real systems, e.g., DAC and MZM, geometrically shaped constellation could perform differently because of their peak-to-average power ratio.

The MI and GMI metrics
Because of high dimensionality and constellations sized for multidimensional constellation, the computation of MI and GMI could be very com-

plex and time consuming. Exploring low-complexity methods to estimate these metrics is an interesting research topic for future works.

Efficient bit labeling
The performance of lattice-based constellations has been investigated in terms of BER in this thesis and natural and quasi-Qray bit labeling have been used to label the symbols. Finding better bit labeling for these constellations by applying machine learning techniques can be considered for more improvements.

Comparison with probabilistic shaping methods
A comprehensive comparison between multidimensional geometric shaping and probabilistic shaping can determine the advantages and disadvantages of each methods in different operation regimes. Implementation complexity of these methods is also an important aspect which can affect the power consumption of the optical systems.

CHAPTER 6

Summary of papers

Paper A
Low-complexity geometric shaping
Journal of Lightwave Technology, vol. 39, no. 2, pp. 363-371, Jan 2021.

In this paper, we have investigated the performance of multidimensional geometric shaping based on lattices. Fast and low-complexity algorithms have been used to make the transmission and detection of high-cardinality constellations possible. Simulations have been done over the linear AWGN and nonlinear fiber optic channels using the split-step Fourier method. Two low-complexity bit labeling approaches have been studied to explore the uncoded BER. Over the nonlinear fiber channel, we demonstrate more than 38% reach improvements compared to 4-QAM.

Paper B
Lattice-based geometric shaping
European Conference on Optical Communication (ECOC), Brussels, Belgium, Dec 2020.

Similar to [Paper A], lattice-based constellations have been investigated, but here in terms of SER without considering the bit labeling. The multidimensional constellations have been realized using frequency, polariza-

tions, and IQ components. We demonstrate more than 78% transmission reach and 4.5 dB power improvements compared to uniform QAM formats at the same normalized symbol error rate.

Paper C
Comparison of uniform cross QAM and probabilistically shaped QAM formats under the impact of transmitter impairments
European Conference on Optical Communication (ECOC), Dublin, Ireland, Sep 2019.

In this paper, the impact of transmitter impairments including the DAC and MZM are explored for probabilistically shaped QAM and cross-QAM constellations. The fiber channel is considered as an AWGN channel. We demonstrate that cross-QAM outperforms PS-QAM by a factor of up to 4 in symbol error rate and higher achievable information rates, at the same source entropy and optimal electrical signal powers.

Paper D
Performance of probabilistic shaping coherent channels in hybrid systems
International Conference on Transparent Optical Networks (ICTON), Bari, Italy, July 2020.

In this paper, the performance of probabilistically shaped QAM formats is compared with uniform QAM in links where higher order modulation formats co-propagate with OOK channels. The results show that increasing the number of OOK channels, increases the nonlinear effects on the coherent channels and the performance of uniform QAM formats degrade faster compared to probabilistically shaped QAM.

References

[1] M. Douglas, S. V. Katikireddi, M. Taulbut, M. McKee, and G. McCartney, "Mitigating the wider health effects of COVID-19 pandemic response," *BMJ*, vol. 369, 2020.

[2] R. M. del Rio-Chanona, P. Mealy, A. Pichler, F. Lafond, and J. D. Farmer, "Supply and demand shocks in the COVID-19 pandemic: An industry and occupation perspective," *Oxford Review of Economic Policy*, vol. 36, no. Supplement_1, pp. S94–S137, 2020.

[3] J. Daniel, "Education and the COVID-19 pandemic," *Prospects*, vol. 49, no. 1, pp. 91–96, 2020.

[4] C. Rose, S. Mott, A. Alvarez, and M. Lin, "Physically distant, educationally connected: interactive conferencing in the era of COVID-19," *Medical education*, vol. 54, no. 8, pp. 758–759, 2020.

[5] A. Feldmann, O. Gasser, F. Lichtblau, E. Pujol, I. Poese, C. Dietzel, D. Wagner, M. Wichtlhuber, J. Tapiador, N. Vallina-Rodriguez *et al.*, "The Lockdown Effect: Implications of the COVID-19 Pandemic on Internet Traffic," in *Proceedings of the ACM Internet Measurement Conference*, 2020, pp. 1–18.

[6] M. Candela, V. Luconi, and A. Vecchio, "Impact of the COVID-19 pandemic on the Internet latency: A large-scale study," *Computer Networks*, vol. 182, p. 107495, 2020.

[7] R. Hui, *Introduction to fiber-optic communications.* Academic Press, 2019.

[8] A. L. Schawlow and C. H. Townes, "Infrared and optical masers," *Physical Review*, vol. 112, no. 6, p. 1940, 1958.

[9] W. Koechner, *Solid-state laser engineering.* Springer, 2013, vol. 1.

[10] H. Murata, *Handbook of optical fibers and cables.* CRC Press, 2020, vol. 1.

[11] T. H. MAIMAN, "Stimulated Optical Radiation in Ruby," *Nature*, vol. 187, no. 4736, pp. 493–494, Aug 1960. [Online]. Available: https://doi.org/10.1038/187493a0

[12] A. Javan, W. R. Bennett Jr, and D. R. Herriott, "Population inversion and continuous optical maser oscillation in a gas discharge containing a He-Ne mixture," *Physical Review Letters*, vol. 6, no. 3, p. 106, 1961.

[13] R. N. Hall, G. E. Fenner, J. Kingsley, T. Soltys, and R. Carlson, "Coherent light emission from GaAs junctions," *Physical Review Letters*, vol. 9, no. 9, p. 366, 1962.

[14] B. I. Hirschowitz, "Photography through the fiber gastroscope," *The American journal of digestive diseases*, vol. 8, no. 5, pp. 389–395, 1963.

[15] F. Kapron, D. B. Keck, and R. D. Maurer, "Radiation losses in glass optical waveguides," *Applied Physics Letters*, vol. 17, no. 10, pp. 423–425, 1970.

[16] R. Csencsits, P. Lemaire, W. Reed, D. Shenk, and K. Walker, "Fabrication of low-loss single-mode fibers," in *Optical Fiber Communication Conference (OFC)*, 1984, p. TuI3.

[17] H. Yokota, H. Kanamori, Y. Ishiguro, G. Tanaka, S. Tanaka, H. Takada, M. Watanabe, S. Suzuki, K. Yano, M. Hoshikawa *et al.*, "Ultra-low-loss pure-silica-core single-mode fiber and transmission experiment," in *Optical Fiber Communication Conference (OFC)*, 1986, p. PD3.

[18] R. Kerdock and D. Wolaver, "Atlanta fiber system experiment: results of the atlanta experiment," *Bell System Technical Journal*, vol. 57, no. 6, pp. 1857–1879, 1978.

[19] I. Jacobs, "Atlanta fiber system experiment: Overview," *Bell System Technical Journal*, vol. 57, no. 6, pp. 1717–1721, 1978.

[20] R. J. Mears, L. Reekie, I. Jauncey, and D. N. Payne, "Low-noise erbium-doped fibre amplifier operating at 1.54 μm," *Electronics Letters*, vol. 23, no. 19, pp. 1026–1028, 1987.

[21] J. M. Simmons, *Optical network design and planning.* Springer, 2014.

[22] C.-H. Yeh, C.-C. Lee, and S. Chi, "120-nm bandwidth erbium-doped fiber amplifier in parallel configuration," *IEEE Photonics Technology Letters*, vol. 16, no. 7, pp. 1637–1639, 2004.

[23] G. P. Agrawal, "Optical communication: its history and recent progress," in *Optics in our time.* Springer, Cham, 2016.

[24] S. Tsukamoto, D.-S. Ly-Gagnon, K. Katoh, and K. Kikuchi, "Coherent demodulation of 40-Gbit/s polarization-multiplexed QPSK signals with 16-GHz spacing after 200-km transmission," in *Optical Fiber Communication Conference (OFC)*, 2005, p. PDP29.

[25] P. J. Winzer and R.-J. Essiambre, "Advanced optical modulation formats," *Optical Fiber Telecommunications VB*, pp. 23–93, 2008.

[26] C. E. Shannon, "A mathematical theory of communication," *Bell system technical journal*, vol. 27, no. 3, pp. 379–423, 1948.

[27] R.-J. Essiambre, G. Kramer, P. J. Winzer, G. J. Foschini, and B. Goebel, "Capacity limits of optical fiber networks," *Journal of Lightwave Technology*, vol. 28, no. 4, pp. 662–701, 2010.

[28] E. Agrell, A. Alvarado, G. Durisi, and M. Karlsson, "Capacity of a nonlinear optical channel with finite memory," *Journal of Lightwave Technology*, vol. 32, no. 16, pp. 2862–2876, 2014.

[29] E. Agrell, "Conditions for a monotonic channel capacity," *IEEE Transactions on Communications*, vol. 63, no. 3, pp. 738–748, 2014.

[30] ——, "Nonlinear fiber capacity," in *European Conference and Exhibition on Optical Communication (ECOC)*, 2013.

[31] H. Dzieciol, G. Liga, E. Sillekens, P. Bayvel, and D. Lavery, "Geometric Shaping of 2-D Constellations in the Presence of Laser Phase Noise," *Journal of Lightwave Technology*, vol. 39, no. 2, pp. 481–490, 2020.

[32] B. Chen, Y. Lei, D. Lavery, C. Okonkwo, and A. Alvarado, "Rate-adaptive coded modulation with geometrically-shaped constellations," in *2018 Asia Communications and Photonics Conference (ACP)*, 2018.

[33] T. Fehenberger, A. Alvarado, G. Böcherer, and N. Hanik, "On probabilistic shaping of quadrature amplitude modulation for the nonlinear fiber channel," *Journal of Lightwave Technology*, vol. 34, no. 21, pp. 5063–5073, 2016.

[34] T. Fehenberger, "Information rates of probabilistically shaped coded modulation for a multi-span fiber-optic communication system with 64qam," *Optics Communications*, vol. 409, pp. 2–6, 2018.

[35] I. F. de Jauregui Ruiz, A. Ghazisaeidi, O. A. Sab, P. Plantady, A. Calsat, S. Dubost, L. Schmalen, V. Letellier, and J. Renaudier, "25.4-Tb/s transmission over transpacific distances using truncated probabilistically shaped PDM-64QAM," *Journal of Lightwave Technology*, vol. 36, no. 6, pp. 1354–1361, 2018.

[36] J.-X. Cai, H. Batshon, M. V. Mazurczyk, O. V. Sinkin, D. Wang, M. Paskov, W. Patterson, C. R. Davidson, P. Corbett, G. Wolter *et al.*, "70.4 Tb/s capacity over 7,600 km in C+ L band using coded modulation with hybrid constellation shaping and nonlinearity compensation," in *Optical Fiber Communication Conference (OFC)*, 2017, pp. Th5B–2.

[37] J.-X. Cai, H. G. Batshon, M. V. Mazurczyk, O. V. Sinkin, D. Wang, M. Paskov, C. R. Davidson, W. W. Patterson, A. Turukhin, M. A. Bolshtyansky *et al.*, "51.5 tb/s capacity over 17,107 km in c+ l bandwidth using single-mode fibers and nonlinearity compensation," *Journal of Lightwave Technology*, vol. 36, no. 11, pp. 2135–2141, 2018.

[38] T. Kanada, Y. Okano, K. Aoyama, and T. Kitami, "Design and performance of wdm transmission systems at 6.3 mbits/s," *IEEE transactions on communications*, vol. 31, no. 9, pp. 1095–1102, 1983.

[39] F. Buchali, V. Aref, M. Chagnon, K. Schuh, H. Hettrich, A. Bielik, L. Altenhain, M. Guntermann, R. Schmid, and M. Moller, "1.52 Tb/s single carrier transmission supported by a 128 GSa/s SiGe DAC," in *Optical Fiber Communication Conference (OFC)*, 2020, pp. Th4C–2.

[40] M. Mazur, J. Schröder, A. Lorences-Riesgo, T. Yoshida, M. Karlsson, and P. A. Andrekson, "11.5 bits/s/Hz PM-256QAM comb-based superchannel transmission by combining optical and digital pilots," in *Optical Fiber Communications Conference (OFC)*, 2018.

[41] S. J. Savory and D. S. Millar, "DSP for Optical Transponders," in *Springer Handbook of Optical Networks*. Springer, 2020, pp. 155–176.

[42] J. C. Rasmussen, T. Takahara, T. Tanaka, Y. Kai, M. Nishihara, T. Drenski, L. Li, W. Yan, and Z. Tao, "Digital signal processing for short reach optical links," in *European Conference on Optical Communication (ECOC)*, 2014.

[43] D. A. Huffman, "A method for the construction of minimum-redundancy codes," *Proceedings of the IRE*, vol. 40, no. 9, pp. 1098–1101, 1952.

[44] A. G. i Amat and L. Schmalen, "Forward error correction for optical transponders," in *Springer Handbook of Optical Networks*. Springer, 2020, pp. 177–257.

[45] E. Agrell and M. Karlsson, "Power-efficient modulation formats in coherent transmission systems," *Journal of Lightwave Technology*, vol. 27, no. 22, pp. 5115–5126, 2009.

[46] M. Karlsson and E. Agrell, "Four-dimensional optimized constellations for coherent optical transmission systems," in *European Conference on Optical Communication (ECOC)*, 2010.

[47] S. Benedetto and E. Biglieri, *Principles of Digital Transmission: with Wireless Applications*. Springer, 1999.

[48] J. Proakis, *Digital Communications*, ser. Communications and signal processing. McGraw-Hill, 1995.

[49] A. Gorlov, A. Gelgor, and V. P. Nguyen, "Root-raised cosine versus optimal finite pulses for faster-than-Nyquist generation," in *Internet of Things, Smart Spaces, and Next Generation Networks and Systems*. Springer, 2016, pp. 628–640.

[50] M. Joost, "Theory of root-raised cosine filter," *Research and Development*, vol. 47829, 2010.

[51] P. Gou, L. Zhao, K. Wang, W. Zhou, and J. Yu, "Nonlinear look-up table predistortion and chromatic dispersion precompensation for IM/DD PAM-4 transmission," *IEEE Photonics Journal*, vol. 9, no. 5, 2017.

[52] K. Roberts, C. Li, L. Strawczynski, M. O'Sullivan, and I. Hardcastle, "Electronic precompensation of optical nonlinearity," *IEEE Photonics Technology Letters*, vol. 18, no. 2, pp. 403–405, 2006.

[53] A. Napoli, P. W. Berenguer, T. Rahman, G. Khanna, M. M. Mezghanni, L. Gardian, E. Riccardi, A. C. Piat, S. Calabrò, S. Dris *et al.*, "Digital pre-compensation techniques enabling high-capacity bandwidth variable transponders," *Optics Communications*, vol. 409, pp. 52–65, 2018.

[54] C. Schmidt, C. Kottke, V. Jungnickel, and R. Freund, "High-speed digital-to-analog converter concepts," in *Next-Generation Optical Communication: Components, Sub-Systems, and Systems VI*, vol. 10130. International Society for Optics and Photonics, 2017, p. 101300N.

[55] C. Laperle and M. O'Sullivan, "Advances in high-speed DACs, ADCs, and DSP for optical coherent transceivers," *Journal of lightwave technology*, vol. 32, no. 4, pp. 629–643, 2014.

[56] D. Rafique, A. Napoli, S. Calabro, and B. Spinnler, "Digital preemphasis in optical communication systems: On the DAC requirements for terabit transmission applications," *Journal of Lightwave Technology*, vol. 32, no. 19, pp. 3247–3256, 2014.

[57] A. Napoli, M. M. Mezghanni, T. Rahman, D. Rafique, R. Palmer, B. Spinnler, S. Calabrò, C. Castro, M. Kuschnerov, and M. Bohn,

"Digital compensation of bandwidth limitations for high-speed DACs and ADCs," *Journal of Lightwave Technology*, vol. 34, no. 13, pp. 3053–3064, 2016.

[58] K. Kikuchi, "Fundamentals of coherent optical fiber communications," *Journal of Lightwave Technology*, vol. 34, no. 1, pp. 157–179, 2015.

[59] A. Napoli, M. M. Mezghanni, D. Rafique, V. A. Sleiffer, B. Spinnler, and M. Bohn, "Novel digital pre-distortion techniques for low-extinction ratio Mach-Zehnder modulators," in *Optical Fiber Communication Conference (OFC)*, 2015, pp. Th3G–1.

[60] D. Rafique, H. Griesser, and J.-P. Elbers, "Enabling 64Gbaud coherent optical transceivers," in *Optical Fiber Communications Conference(OFC)*, 2017.

[61] A. F. Alfredsson, E. Agrell, and H. Wymeersch, "Iterative detection and phase-noise compensation for coded multichannel optical transmission," *IEEE Transactions on Communications*, vol. 67, no. 8, pp. 5532–5543, 2019.

[62] D. Villafani, A. Mirani, X. Pang, E. Goobar, J. Schröder, M. Karlsson, and P. Andrekson, "Phase Noise Characterization and EEPN of a Full C-Band Tunable Laser in Coherent Optical Systems," *IEEE Photonics Technology Letters*, vol. 31, no. 24, pp. 1991–1994, 2019.

[63] Z. Jia, H.-C. Chien, J. Zhang, Z. Dong, and Y. Cai, "Performance analysis of pre-and post-compensation for bandwidth-constrained signal in high-spectral-efficiency optical coherent systems," in *Optical Fiber Communication Conference (OFC)*, 2014.

[64] I. Fatadin, S. J. Savory, and D. Ives, "Compensation of quadrature imbalance in an optical QPSK coherent receiver," *IEEE Photonics Technology Letters*, vol. 20, no. 20, pp. 1733–1735, 2008.

[65] A. B. Dar and R. K. Jha, "Chromatic dispersion compensation techniques and characterization of fiber Bragg grating for dispersion compensation," *Optical and Quantum Electronics*, vol. 49, no. 3, p. 108, 2017.

[66] S. J. Savory, G. Gavioli, R. I. Killey, and P. Bayvel, "Electronic compensation of chromatic dispersion using a digital coherent receiver," *Optics express*, vol. 15, no. 5, pp. 2120–2126, 2007.

[67] F. Gardner, "A BPSK/QPSK timing-error detector for sampled receivers," *IEEE Transactions on communications*, vol. 34, no. 5, pp. 423–429, 1986.

[68] S. J. Savory, "Digital coherent optical receivers: Algorithms and subsystems," *IEEE Journal of selected topics in quantum electronics*, vol. 16, no. 5, pp. 1164–1179, 2010.

[69] M. Mazur, J. Schröder, A. Lorences-Riesgo, T. Yoshida, M. Karlsson, and P. A. Andrekson, "Overhead-optimization of pilot-based digital signal processing for flexible high spectral efficiency transmission," *Optics express*, vol. 27, no. 17, pp. 24 654–24 669, 2019.

[70] E. Ip and J. M. Kahn, "Compensation of dispersion and nonlinear impairments using digital backpropagation," *Journal of Lightwave Technology*, vol. 26, no. 20, pp. 3416–3425, 2008.

[71] T. Sasaki, T. Hasegawa, and H. Ishikawa, "Optical fiber and cables," *Springer Handbook of Optical Networks*, pp. 25–49, 2020.

[72] G. P. Agrawal, *Nonlinear Fiber Optics*, 5th ed. Springer, 2013.

[73] T. A. Eriksson, T. Fehenberger, P. A. Andrekson, M. Karlsson, N. Hanik, and E. Agrell, "Impact of 4D channel distribution on the achievable rates in coherent optical communication experiments," *Journal of Lightwave Technology*, vol. 34, no. 9, pp. 2256–2266, 2016.

[74] S. Mumtaz, R.-J. Essiambre, and G. P. Agrawal, "Nonlinear propagation in multimode and multicore fibers: Generalization of the Manakov equations," *Journal of Lightwave Technology*, vol. 31, no. 3, pp. 398–406, 2012.

[75] C. Antonelli, M. Shtaif, and A. Mecozzi, "Modeling of nonlinear propagation in space-division multiplexed fiber-optic transmission," *Journal of Lightwave Technology*, vol. 34, no. 1, pp. 36–54, 2015.

[76] S. Li, M. Karlsson, and E. Agrell, "Improved simulation accuracy of the split-step fourier method," in *Optical Fiber Communication Conference (OFC)*, 2020, pp. W2A–55.

[77] P. Poggiolini, "The GN model of non-linear propagation in uncompensated coherent optical systems," *Journal of Lightwave Technology*, vol. 30, no. 24, pp. 3857–3879, 2012.

[78] E. Agrell, G. Durisi, and P. Johannisson, "Information-theory-friendly models for fiber-optic channels: A primer," in *Information Theory Workshop (ITW)*, 2015.

[79] E. Agrell, M. Karlsson, A. Chraplyvy, D. J. Richardson, P. M. Krummrich, P. Winzer, K. Roberts, J. K. Fischer, S. J. Savory, B. J. Eggleton *et al.*, "Roadmap of optical communications," *Journal of Optics*, vol. 18, no. 6, p. 063002, 2016.

[80] P. J. Winzer, "High-spectral-efficiency optical modulation formats," *Journal of Lightwave Technology*, vol. 30, no. 24, pp. 3824–3835, 2012.

[81] M. Karlsson and E. Agrell, "Multidimensional Modulation and Coding in Optical Transport," *Journal of Lightwave Technology*, vol. 35, no. 4, pp. 876–884, 2016.

[82] D. S. Millar, T. Koike-Akino, S. Ö. Arık, K. Kojima, K. Parsons, T. Yoshida, and T. Sugihara, "High-dimensional modulation for coherent optical communications systems," *Optics Express*, vol. 22, no. 7, pp. 8798–8812, 2014.

[83] T. A. Eriksson, P. Johannisson, E. Agrell, P. A. Andrekson, and M. Karlsson, "Biorthogonal modulation in 8 dimensions experimentally implemented as 2PPM-PS-QPSK," in *Optical Fiber Communication Conference (OFC)*, 2014.

[84] S. J. Savory, "Digital signal processing options in long haul transmission," in *Optical Fiber Communication Conference (OFC)*, 2008, p. OTuO3.

[85] Z. Qu, I. B. Djordjevic, and J. Anderson, "Two-dimensional constellation shaping in fiber-optic communications," *Applied sciences*, vol. 9, no. 9, p. 1889, 2019.

[86] D. Pilori, A. Nespola, F. Forghieri, and G. Bosco, "Non-linear phase noise mitigation over systems using constellation shaping," *Journal of Lightwave Technology*, vol. 37, no. 14, pp. 3475–3482, 2019.

[87] J. H. Conway and N. J. A. Sloane, *Sphere Packings, Lattices and Groups*, 3rd ed. Springer, 1999.

[88] M. Karlsson and E. Agrell, "Power-efficient modulation schemes," in *Impact of Nonlinearities on Fiber Optic Communications*. Springer, 2011, pp. 219–252.

[89] ——, "Spectrally efficient four-dimensional modulation," in *Optical Fiber Communications Conference (OFC)*, 2012.

[90] K. Onohara, T. Sugihara, Y. Miyata, K. Sugihara, K. Kubo, H. Yoshida, K. Koguchi, and T. Mizuochi, "Soft-decision forward error correction for 100 Gb/s digital coherent systems," *Optical Fiber Technology*, vol. 17, no. 5, pp. 452–455, 2011.

[91] A. Alvarado, E. Agrell, D. Lavery, R. Maher, and P. Bayvel, "Replacing the soft-decision fec limit paradigm in the design of optical communication systems," *Journal of Lightwave Technology*, vol. 33, no. 20, pp. 4338–4352, 2015.

[92] A. Alvarado, T. Fehenberger, B. Chen, and F. M. Willems, "Achievable information rates for fiber optics: Applications and computations," *Journal of Lightwave Technology*, vol. 36, no. 2, pp. 424–439, 2018.

[93] U. Wachsmann, R. F. Fischer, and J. B. Huber, "Multilevel codes: Theoretical concepts and practical design rules," *IEEE Transactions on Information Theory*, vol. 45, no. 5, pp. 1361–1391, 1999.

[94] B. P. Smith and F. R. Kschischang, "A pragmatic coded modulation scheme for high-spectral-efficiency fiber-optic communications," *Journal of Lightwave Technology*, vol. 30, no. 13, pp. 2047–2053, 2012.

[95] J. Cho and P. J. Winzer, "Probabilistic constellation shaping for optical fiber communications," *Journal of Lightwave Technology*, vol. 37, no. 6, pp. 1590–1607, 2019.

[96] P. J. Winzer, D. T. Neilson, and A. R. Chraplyvy, "Fiber-optic transmission and networking: the previous 20 and the next 20 years," *Optics Express*, vol. 26, no. 18, pp. 24 190–24 239, 2018.

[97] M. P. Yankov, D. Zibar, K. J. Larsen, L. P. Christensen, and S. Forchhammer, "Constellation shaping for fiber-optic channels with QAM and high spectral efficiency," *IEEE Photonics Technology Letters*, vol. 26, no. 23, pp. 2407–2410, 2014.

[98] R. F. Fischer, *Precoding and signal shaping for digital transmission*. John Wiley & Sons, 2005.

[99] T. M. Cover, *Elements of information theory*. John Wiley & Sons, 1999.

[100] K. Keykhosravi, G. Durisi, and E. Agrell, "Accuracy assessment of nondispersive optical perturbative models through capacity analysis," *Entropy*, vol. 21, no. 8, p. 760, 2019.

[101] H. Iimori, R.-A. Stoica, and G. T. F. de Abreu, "Constellation shaping for rate maximization in AWGN channels with non-linear distortion," in *International Workshop on Computational Advances in Multi-Sensor Adaptive Processing (CAMSAP)*, 2017.

[102] D. Pilori, F. Forghieri, and G. Bosco, "Maximization of the achievable mutual information using probabilistically shaped squared-QAM constellations," in *Optical Fiber Communication Conference (OFC)*, 2017.

[103] L. Schmalen, "Probabilistic constellation shaping: Challenges and opportunities for forward error correction," in *Optical Fiber Communications Conference (OFC)*, 2018.

[104] B. Chen, C. Okonkwo, H. Hafermann, and A. Alvarado, "Increasing achievable information rates via geometric shaping," in *European Conference on Optical Communication (ECOC)*, 2018.

[105] R. T. Jones, M. P. Yankov, and D. Zibar, "End-to-end learning for GMI optimized geometric constellation shape," in *European Conference on Optical Communication (ECOC)*, 2019.

[106] K. Gümüş, A. Alvarado, B. Chen, C. Häger, and E. Agrell, "End-to-End Learning of Geometrical Shaping Maximizing Generalized

Mutual Information," in *Optical Fiber Communications Conference (OFC)*, 2020.

[107] R. T. Jones, T. A. Eriksson, M. P. Yankov, and D. Zibar, "Deep learning of geometric constellation shaping including fiber nonlinearities," in *European Conference on Optical Communication (ECOC)*, 2018.

[108] M. Stark, F. A. Aoudia, and J. Hoydis, "Joint learning of geometric and probabilistic constellation shaping," in *Globecom Workshops (GC Wkshps)*, 2019.

[109] G. D. Forney, Jr., R. G. Gallager, G. R. Lang, F. M. Longstaff, and S. U. Qureshi, "Efficient modulation for band-limited channels," *IEEE Journal on Selected Areas in Communications*, vol. 2, no. 5, pp. 632–647, 1984.

[110] G. D. Forney, Jr., "Multidimensional constellations-Part II. Voronoi constellations," *IEEE Journal on Selected Areas in Communications*, vol. 7, no. 6, pp. 941–958, 1989.

[111] J. Conway and N. Sloane, "A fast encoding method for lattice codes and quantizers," *IEEE Transactions on Information Theory*, vol. 29, no. 6, pp. 820–824, 1983.

Included papers A–D

Paper A

"Low-complexity geometric shaping",
Ali Mirani, Erik Agrell, and Magnus Karlsson,
Journal of Lightwave Technology, vol. 39, no. 2, pp. 363-371, Jan 2021.

Paper B

"Lattice-based geometric shaping",
Ali Mirani, Erik Agrell, and Magnus Karlsson,
European Conference on Optical Communication (ECOC), Brussels, Belgium, Dec 2020.

Paper C

"Comparison of uniform cross QAM and probabilistically shaped QAM formats under the impact of transmitter impairments", **Ali Mirani**, Mikael Mazur, Erik Agrell, Benjamin Foo, Jochen Schröder, Peter Andrekson, and Magnus Karlsson,
European Conference on Optical Communication (ECOC), Dublin, Ireland, Sep 2019.

Paper D

"Performance of Probabilistic Shaping Coherent Channels in Hybrid Systems",
Diego Villafani, **Ali Mirani**, Henrik Åhlfeldt, Jochen Schröder, Magnus Karlsson, and Peter Andrekson,
International Conference on Transparent Optical Networks (ICTON), Bari, Italy, July 2020.